Article

SOURCE DATA | TRANSPARENT PROCESS

THE EMBO JOURNAL

An alternative UPF1 isoform drives conditional remodeling of nonsense-mediated mRNA decay

Sarah E Fritz, Soumya Ranganathan, Clara D Wang & J Robert Hogg*

Abstract

The nonsense-mediated mRNA decay (NMD) pathway monitors translation termination in order to degrade transcripts with premature stop codons and regulate thousands of human genes. Here, we show that an alternative mammalian-specific isoform of the core NMD factor UPF1, termed $UPF1_{LL}$, enables condition-dependent remodeling of NMD specificity. Previous studies indicate that the extension of a conserved regulatory loop in the $UPF1_{LL}$ helicase core confers a decreased propensity to dissociate from RNA upon ATP hydrolysis relative to $UPF1_{SL}$, the major UPF1 isoform. Using biochemical and transcriptome-wide approaches, we find that $UPF1_{LL}$ can circumvent the protective RNA binding proteins PTBP1 and hnRNP L to preferentially bind and down-regulate transcripts with long 3'UTRs normally shielded from NMD. Unexpectedly, $UPF1_{LL}$ supports induction of NMD on new populations of substrate mRNAs in response to activation of the integrated stress response and impaired translation efficiency. Thus, while canonical NMD is abolished by moderate translational repression, $UPF1_{LL}$ activity is enhanced, offering the possibility to rapidly rewire NMD specificity in response to cellular stress.

Keywords hnRNP L; nonsense-mediated mRNA decay; PTBP1; translation termination; UPF1

Subject Categories Translation & Protein Quality

DOI 10.15252/embj.2021108898 | Received 7 June 2021 | Revised 18 March 2022 | Accepted 25 March 2022 | Published online 11 April 2022

The EMBO Journal (2022) 41: e108898

Introduction

Nonsense-mediated mRNA decay (NMD) is an evolutionarily conserved mRNA quality-control pathway that degrades transcripts undergoing premature translation termination (Smith & Baker, 2015; Lavysh & Neu-Yilik, 2020). In addition, NMD performs a regulatory role by governing the turnover of ~5–10% of the transcriptome, including mRNAs with upstream open reading frames (uORFs), introns downstream of the stop codon, or long 3' untranslated regions (UTRs) (Kishor *et al*, 2019a). Despite extensive studies of the large impact of NMD on the transcriptome, the mechanisms by which the pathway selects its regulatory targets are poorly understood.

A suite of conserved NMD factors acts in concert with general mRNA binding proteins and RNA decay enzymes to identify and degrade target mRNAs. The RNA helicase UPF1 is a central coordinator of the NMD pathway, as it directly binds mRNA and functions at multiple steps in the selection and degradation of target transcripts (Kim & Maquat, 2019). Additional core NMD factors UPF2 and UPF3 promote UPF1 activity and link UPF1 to the exon junction complex (EJC), which strongly stimulates decay (Le Hir *et al*, 2000a, 2000b; Chamieh *et al*, 2008). In many eukaryotes, NMD execution also depends on the SMG1, 5, 6, and 7 proteins (Hodgkin *et al*, 1989; Pulak & Anderson, 1993; Page *et al*, 1999; Causier *et al*, 2017). Phosphorylation of UPF1 by the SMG1 kinase is required for efficient mRNA decay (Kashima *et al*, 2006), as phosphorylated UPF1 recruits the SMG6 endonuclease and/or general decapping and deadenylation enzymes through the SMG5/7 heterodimer (Huntzinger *et al*, 2008; Eberle *et al*, 2009; Loh *et al*, 2013).

In addition to the functions of specialized NMD proteins, substrate selection and degradation by the NMD pathway require the translation termination machinery to detect in-frame stop codons (Karousis & Mühlemann, 2019). Although the molecular details remain to be elucidated, it is widely accepted that interactions between core NMD factors and a terminating ribosome are necessary for decay (Lavysh & Neu-Yilik, 2020). Because of the strict dependence of NMD on translation termination, decay efficiency of canonical NMD targets is expected to be tightly linked to translation efficiency. However, there is evidence that NMD efficiency for some targets is actually enhanced when translation is impaired by treatment with the mTOR inhibitor rapamycin or the translation elongation inhibitor emetine (Martinez-Nunez *et al*, 2017). These data warrant a more extensive investigation into the role of translation in shaping target specificity by the NMD pathway, particularly during changing physiological conditions.

The ability of UPF1 to bind and hydrolyze ATP is critical for the selection and degradation of potential NMD substrates (Franks *et al*, 2010; Kurosaki *et al*, 2014; Lee *et al*, 2015). Numerous studies have provided evidence that the affinity of UPF1 for RNA is reduced by ATP binding and hydrolysis, in a manner dependent on an 11 amino acid regulatory loop in domain 1B of the helicase core that protrudes into the RNA binding channel (Czaplinski *et al*, 1995; Weng *et al*, 1998; Cheng *et al*, 2007; Chamieh *et al*, 2008; Chakrabarti *et al*, 2011; Fiorini *et al*, 2013; Gowravaram *et al*, 2018). Intriguingly, mammals undergo an alternative splicing event to express two UPF1 isoforms that differ only in length of the regulatory loop (Fig 1A).

Biochemistry and Biophysics Center, National Heart, Lung, and Blood Institute, National Institutes of Health, Bethesda, MD, USA
*Correspondence: Tel: +1 301 827 0724; E-mail: j.hogg@nih.gov

Almost all NMD studies to date have focused on the more abundant UPF1 "short loop" isoform (designated herein $UPF1_{SL}$), which contains the 11 amino acid regulatory loop that most potently weakens the affinity of UPF1 for RNA in the presence of ATP. Alternative 5' splice site usage in exon 7 of UPF1 generates a second UPF1 isoform that extends the regulatory loop to 22 amino acids, the sequence of which is conserved among mammals spanning humans to marsupials (Appendix Fig S1A). This naturally occurring UPF1 "long loop" isoform (designated herein $UPF1_{LL}$), which represents ~15–25% of total UPF1 mRNA in diverse cell and tissue types (Appendix Fig S1B), has increased catalytic activity and a higher affinity for RNA in the presence of ATP than the $UPF1_{SL}$ isoform (Gowravaram *et al*, 2018). It is unknown whether the differential biochemical properties of the $UPF1_{LL}$ isoform affect NMD specificity in cells.

Here, we show that the $UPF1_{LL}$ isoform gives the mammalian NMD pathway the latent ability to remodel NMD target specificity in response to changing physiological conditions. We identify that $UPF1_{LL}$ can overcome inhibition by polypyrimidine tract binding protein 1 (PTBP1) and heterogeneous nuclear ribonucleoprotein L (hnRNP L) to preferentially associate with and down-regulate long 3'UTRs normally shielded from NMD. Unexpectedly, we find that $UPF1_{LL}$ activity is sustained or even enhanced in conditions of reduced translation efficiency, including during the integrated stress response. mRNAs subject to $UPF1_{LL}$-dependent downregulation upon translation inhibition include hundreds of mRNAs not normally targeted by NMD, many of which are protected by PTBP1 and hnRNP L. Together, our data support that human cells use the $UPF1_{LL}$ isoform to conditionally alter which mRNAs are selected and degraded by the NMD pathway, expanding the scope of NMD in mammalian gene expression control.

Results

Specific $UPF1_{LL}$ depletion causes alterations in gene expression

To specifically interrogate the cellular functions of the $UPF1_{LL}$ isoform, we developed a siRNA that efficiently degrades $UPF1_{LL}$ mRNA without perturbing the expression of the major $UPF1_{SL}$ isoform (Fig 1B (top) and Fig EV1A). As an initial analysis of $UPF1_{LL}$ functions, we treated human HEK-293 cells with the $UPF1_{LL}$-specific siRNA ($siUPF1_{LL}$) and performed total RNA-seq. Differential expression analysis identified 1621 genes that were at least 1.4-fold more highly expressed upon $UPF1_{LL}$ knockdown, out of a total population of 13,668 genes analyzed, indicating a role for endogenous $UPF1_{LL}$ in gene expression regulation (Dataset EV1). To investigate whether the observed changes in mRNA abundance with $UPF1_{LL}$ knockdown were due to differential decay, we used REMBRANDTS software, which infers changes in mRNA stability based upon differences in the relative abundance of exonic and intronic reads from each gene (Alkallas *et al*, 2017). These analyses supported the hypothesis that increases in gene expression upon $siUPF1_{LL}$ were due to inhibition of mRNA decay (Fig EV1B and Dataset EV1).

To investigate how $UPF1_{LL}$ contributes to overall UPF1 activities in HEK-293 cells, we compared the transcriptome-wide effects of specific $UPF1_{LL}$ depletion and knockdown with a pan-isoform UPF1 siRNA ($siUPF1_{total}$). Of 1,540 genes that were up-regulated at least 1.4-fold upon $siUPF1_{LL}$ treatment and met read count cutoffs in all conditions, 512 overlapped with the 1854 genes more highly expressed upon $siUPF1_{total}$ treatment (Fig 1B (bottom) and Dataset EV2). These data suggest that the $UPF1_{LL}$ isoform substantially contributes to UPF1 activities in HEK-293 cells, despite the $UPF1_{LL}$ mRNA representing only ~15% of UPF1 mRNA in these cells (Fig EV1A).

$UPF1_{LL}$ contributes to NMD under normal cellular conditions

We expected that only a subset of genes induced by $siUPF1_{total}$ would be affected by $UPF1_{LL}$, a prediction borne out by the 1,342 genes (72%) that were uniquely up-regulated in the $siUPF1_{total}$ condition. However, we also found that 1,028 genes were up-regulated more than 1.4-fold upon $siUPF1_{LL}$ but not $siUPF1_{total}$ treatment (Fig 1B). Because the existence of a large class of genes regulated by $siUPF1_{LL}$ but not $siUPF1_{total}$ was unexpected, we pursued three strategies to evaluate whether these genes represent genuine $siUPF1_{LL}$ targets: (i) investigation of NMD autoregulation in $siUPF1_{LL}$ and

Figure 1. Alternative $UPF1_{LL}$ splice isoform contributes to NMD under normal cellular conditions.

A (Top) Schematic representation of alternative 5' splice site usage in exon 7 of mammalian UPF1 that results in two UPF1 protein isoforms that differ in length of the regulatory loop within the helicase core. (Bottom) Ribbon diagram of human $UPF1_{SL}$ helicase core overlaid with that of human $UPF1_{LL}$. The regulatory loop in domain 1B is indicated for $UPF1_{SL}$ (light blue) and $UPF1_{LL}$ (purple), based on Protein Data Bank accessions 2XZP and 6EJ5 (Chakrabarti *et al*, 2011; Gowravaram *et al*, 2018).

B (Top) Semiquantitative RT–PCR of $UPF1_{SL}$ or $UPF1_{LL}$ transcript levels following transfection of HEK-293 cells with a NT siRNA or a siRNA that specifically targets the $UPF1_{LL}$ isoform. *(Bottom)* Venn diagram (to scale) of overlapping targets identified from RNA-seq following total UPF1 or $UPF1_{LL}$-specific knockdown. Depicted are genes that increased in abundance at least 1.4-fold (FDR < 0.05) and met read count cutoffs in both datasets. *P*-value indicates enrichment of genes that increased in abundance at least 1.4-fold (FDR < 0.05) with $UPF1_{LL}$-specific knockdown among those regulated by total UPF1, as determined by Fisher's exact test.

C Heat map of changes in relative mRNA abundance for genes encoding NMD factors, as determined from RNA-seq following transfection of HEK-293 cells with a siRNA that targets both UPF1 isoforms ($UPF1_{total}$) or a siRNA that specifically targets the $UPF1_{LL}$ isoform.

D Density plot of changes in relative mRNA abundance as determined by RNA-seq in $SMG7^{ko}/SMG6^{kd}$ cells, relative to a parental cell line treated with control siRNAs (Boehm *et al*, 2021). Genes were categorized as up-regulated by $siUPF1_{total}$ only, $siUPF1_{LL}$ only, or both $siUPF1_{total}$ and $siUPF1_{LL}$. Statistical significance was determined by K–W test, with Dunn's correction for multiple comparisons.

E RT–qPCR analysis of indicated transcripts following transfection of HEK-293 cells with the indicated siRNAs. Relative fold changes are in reference to NT siRNA. Asterisk (*) indicates $P < 0.05$, as determined by two-way ANOVA. Black dots represent individual data points and error bars indicate mean ± SD ($n = 3$ biological replicates). Dashed line indicates $\log_2$(fold change) of +0.5. PTC^+ indicates the use of primers specific to transcript isoforms with validated poison exons (Lareau *et al*, 2007; Ni *et al*, 2007). See also Dataset EV3 for *P*-values associated with each statistical comparison.

F Gene ontology analysis of 1621 genes that increased in expression at least 1.4-fold upon $UPF1_{LL}$-specific knockdown in HEK-293 cells under normal cellular conditions. Genes may map to multiple categories.

Source data are available online for this figure.

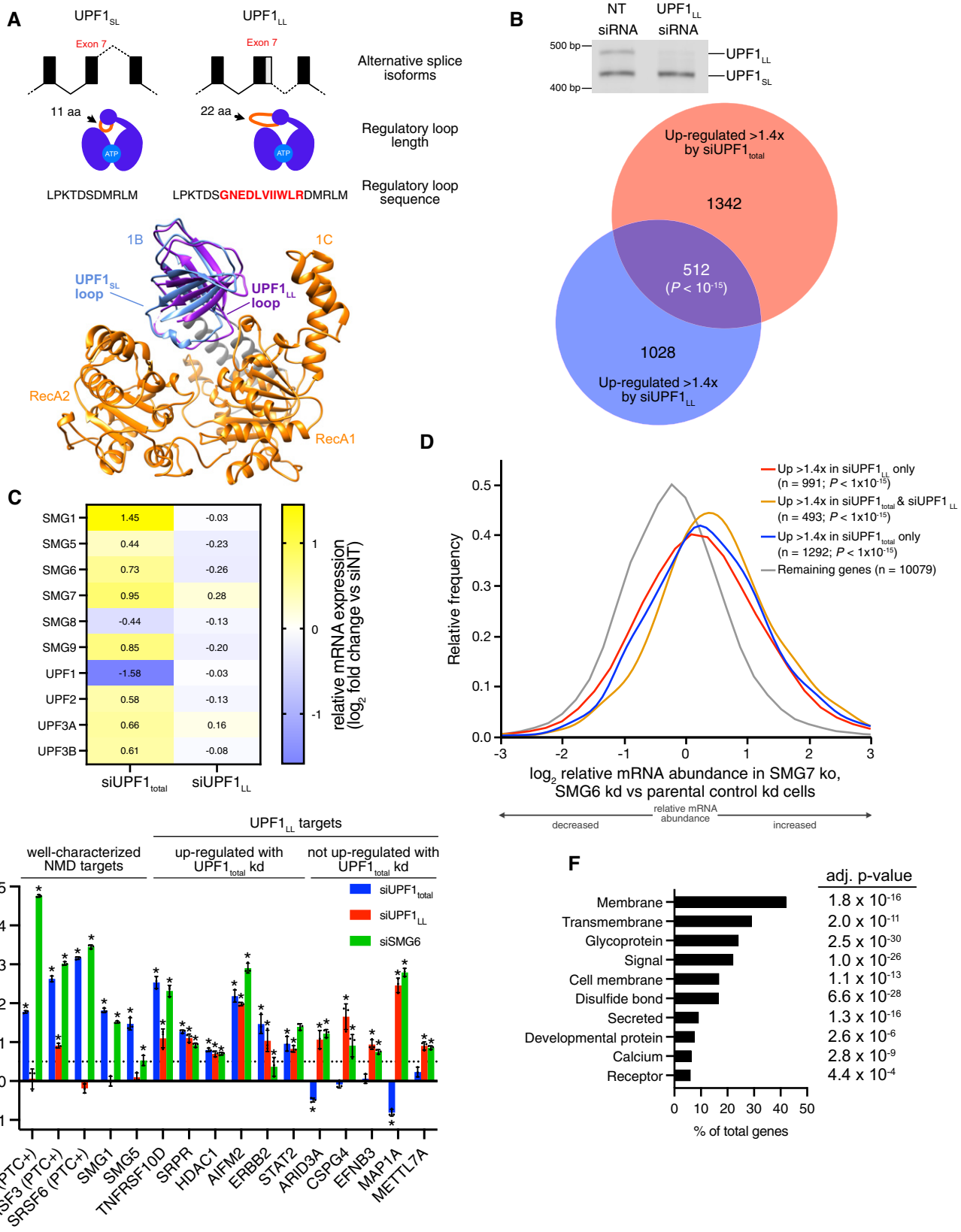
A
UPF1SL
UPF1LL
Exon 7
Exon 7
11 aa
22 aa
ATP
ATP
Alternative splice isoforms
Regulatory loop length
LPKTDSDMRLM
LPKTDSGNEDLVIIWLRDMRLM
Regulatory loop sequence
1B
1C
UPF1SL loop
UPF1LL loop
RecA2
RecA1
B
NT siRNA
UPF1LL siRNA
500 bp
400 bp
UPF1LL
UPF1SL
Up-regulated >1.4x by siUPF1total
1342
512 (P < 10-15)
1028
Up-regulated >1.4x by siUPF1LL
C
SMG1 1.45 -0.03
SMG5 0.44 -0.23
SMG6 0.73 -0.26
SMG7 0.95 0.28
SMG8 -0.44 -0.13
SMG9 0.85 -0.20
UPF1 -1.58 -0.03
UPF2 0.58 -0.13
UPF3A 0.66 0.16
UPF3B 0.61 -0.08
siUPF1total
siUPF1LL
1
0
-1
relative mRNA expression (log2 fold change vs siNT)
D
Up >1.4x in siUPF1LL only (n = 991; P < 1x10-15)
Up >1.4x in siUPF1total & siUPF1LL (n = 493; P < 1x10-15)
Up >1.4x in siUPF1total only (n = 1292; P < 1x10-15)
Remaining genes (n = 10079)
Relative frequency
0.5
0.4
0.3
0.2
0.1
0.0
-3
-2
-1
0
1
2
3
log2 relative mRNA abundance in SMG7 ko, SMG6 kd vs parental control kd cells
relative mRNA abundance
decreased
increased
E
UPF1LL targets
well-characterized NMD targets
up-regulated with UPF1total kd
not up-regulated with UPF1total kd
siUPF1total
siUPF1LL
siSMG6
log2(relative mRNA abundance)
5
4
3
2
1
0
-1
SRSF2 (PTC+)
SRSF3 (PTC+)
SRSF6 (PTC+)
SMG1
SMG5
TNFRSF10D
SRPR
HDAC1
AIFM2
ERBB2
STAT2
ARID3A
CSPG4
EFNB3
MAP1A
METTL7A
F
adj. p-value
Membrane 1.8 x 10-16
Transmembrane 2.0 x 10-11
Glycoprotein 2.5 x 10-30
Signal 1.0 x 10-26
Cell membrane 1.1 x 10-13
Disulfide bond 6.6 x 10-28
Secreted 1.3 x 10-16
Developmental protein 2.6 x 10-6
Calcium 2.8 x 10-9
Receptor 4.4 x 10-4
0
10
20
30
40
50
% of total genes

Figure 1.

siUPF1$_{total}$ conditions, (ii) comparison to additional published NMD RNA-seq datasets, and (iii) analysis of mRNA abundance from cells depleted of UPF1$_{total}$, UPF1$_{LL}$, or SMG6 by RT–qPCR.

The NMD pathway is governed by a conserved autoregulatory program in which depletion or inactivation of NMD pathway components drives elevated expression of several core NMD factors. NMD feedback regulation has been shown to heavily depend on long 3'UTR-dependent turnover of NMD factor mRNAs (Singh *et al*, 2008; Huang *et al*, 2011; Yepiskoposyan *et al*, 2011). In siUPF1$_{total}$ RNA-seq, we observed pathway-wide induction of NMD factor mRNAs, with expression of mRNAs encoding SMG1, SMG6, SMG7, SMG9, UPF2, UPF3A, and UPF3B all increased at least 1.4-fold (Fig 1C). In contrast, UPF1$_{LL}$ depletion had a minimal impact on NMD factor mRNA expression, failing to perturb any by more than 1.2-fold. In an independent experiment, we knocked down UPF1$_{total}$ or UPF1$_{LL}$ and evaluated NMD factor mRNAs by RT–qPCR, again observing up-regulation of NMD factor mRNAs upon siUPF1$_{total}$ but not siUPF1$_{LL}$ treatment (Fig EV1C and Dataset EV3). The finding that UPF1$_{total}$ but not UPF1$_{LL}$ depletion induced compensatory up-regulation of NMD components provides a mechanism to explain why some mRNAs might be de-repressed by UPF1$_{LL}$ knockdown (which does not induce compensatory feedback regulation of NMD) but not by UPF1$_{total}$ knockdown (which induces up-regulation of several core NMD factors).

To further evaluate the contribution of UPF1$_{LL}$ to cellular NMD, we compared our UPF1$_{LL}$-knockdown RNA-seq dataset with a published catalog of high-confidence NMD targets (Colombo *et al*, 2017). Consistent with the overlap between siUPF1$_{LL}$ and siUPF1$_{total}$ in our RNA-seq studies, we observed significant overlaps among the population of genes induced by UPF1$_{LL}$ depletion and those previously determined to be repressed by UPF1, SMG6, or SMG7 (Fig EV1D), with 618 of the putative UPF1$_{LL}$ targets represented in the published NMD target catalog.

Co-regulation of UPF1$_{LL}$ target mRNAs by SMG6

To gain insight into the involvement of other NMD pathway components in UPF1$_{LL}$-dependent regulation, we took advantage of a recently published RNA-seq dataset from experiments in which the Gehring laboratory combined CRISPR-mediated SMG7 knockouts with RNAi-mediated SMG5 or SMG6 knockdowns (Boehm *et al*, 2021). For these analyses, we categorized genes as up-regulated by siUPF1$_{total}$ only, siUPF1$_{LL}$ only, or both siUPF1$_{total}$ and siUPF1$_{LL}$. All three classes exhibited significantly enhanced expression in SMG7^{ko}/SMG6^{kd} cells, relative to a parental cell line treated with control siRNAs (Fig 1D). The greatest degree of up-regulation in SMG7^{ko}/SMG6^{kd} cells was observed for genes induced by both siUPF1$_{total}$ and siUPF1$_{LL}$. Genes that responded to only siUPF1$_{LL}$ were up-regulated in SMG7^{ko}/SMG6^{kd} cells to a very similar extent to those that responded to only siUPF1$_{total}$.

Interestingly, genes induced by siUPF1$_{LL}$ but not siUPF1$_{total}$ exhibited distinct responses to SMG5 depletion in the SMG7^{ko} background. In contrast to the systematic up-regulation of the siUPF1$_{LL}$-only class of genes in SMG7^{ko}/SMG6^{kd} cells, this group of genes was not on average induced in SMG7^{ko}/SMG5^{kd} cells (Fig EV1E). Reciprocally, genes that were up-regulated in SMG7^{ko}/SMG6^{kd} but not SMG7^{ko}/SMG5^{kd} cells were most substantially induced by UPF1$_{LL}$ depletion (Fig EV1F). Together, these analyses support the idea that many genes uniquely up-regulated by siUPF1$_{LL}$ are genuine NMD pathway targets, as they are responsive to co-inactivation of NMD factors SMG6 and SMG7. Moreover, these data suggest that these genes, as a class, are particularly dependent on SMG6 for proper regulation.

To corroborate the results of our own and published RNA-seq datasets, we selected representative genes for evaluation by RT–qPCR of mRNA from cells depleted of UPF1$_{total}$, UPF1$_{LL}$, or SMG6 (Fig 1E and Dataset EV3). We analyzed genes from three major categories: (i) well-characterized NMD targets, including EJC-stimulated alternative splice isoforms of SRSF2, SRSF3, and SRSF6 and long 3'UTR decay targets SMG1 and SMG5, (ii) putative UPF1$_{LL}$ targets regulated by both UPF1$_{LL}$ and UPF1$_{total}$ depletion in our RNA-seq studies, and (iii) putative UPF1$_{LL}$ targets up-regulated by UPF1$_{LL}$ depletion but not UPF1$_{total}$ depletion. Knockdown of UPF1$_{LL}$ had no effect on the levels of well-characterized premature termination codon (PTC)-containing SRSF2 and SRSF6 transcripts, and increased SRSF3 PTC transcript levels to a much smaller extent (~1.9-fold) than total UPF1 (~6.2-fold) or SMG6 (~8.1-fold) knockdown (Lareau *et al*, 2007; Ni *et al*, 2007). Transcriptome-wide, we found a similar pattern, as depletion of UPF1$_{total}$ but not UPF1$_{LL}$ caused systematically elevated expression of PTC-containing transcript isoforms relative to control PTC-free isoforms (Appendix Fig S1C). Importantly, all selected UPF1$_{LL}$ target mRNAs, irrespective of siUPF1$_{total}$ responsiveness, were significantly up-regulated by SMG6 depletion (Fig 1E). These data further reinforce the conclusion that genes responding to UPF1$_{LL}$ but not UPF1$_{total}$ were likely up-regulated due to UPF1$_{LL}$ depletion rather than off-target effects.

Targets of UPF1$_{LL}$ are enriched for ER-associated gene products

The set of genes that respond to siUPF1$_{LL}$ but not siUPF1$_{total}$ is an interesting class because their regulation can be unambiguously attributed to UPF1$_{LL}$ and they can be studied in the absence of the overall NMD pathway up-regulation that results from knockdown of total UPF1 and other NMD factors. However, it is important to note that we do not currently know the mechanisms that determine whether mRNAs regulated by UPF1$_{LL}$ are responsive to siUPF1$_{LL}$ alone or both siUPF1$_{LL}$ and siUPF1$_{total}$, as transcripts uniquely affected by siUPF1$_{LL}$ did not show any significant enrichment for specific NMD-inducing features like PTCs, uORFs, or long 3'UTRs (Appendix Table S1). Therefore, except where noted, further analyses treat the entire population of siUPF1$_{LL}$-responsive genes as putative UPF1$_{LL}$ targets, irrespective of the effects of UPF1$_{total}$ knockdown.

Because genes in functionally related pathways are often coordinately regulated at the posttranscriptional level (Keene, 2007), we performed a gene ontology (GO) enrichment analysis (Eden *et al*, 2009) to identify commonalities among UPF1$_{LL}$ targets. This analysis revealed a high degree of enrichment among UPF1$_{LL}$ targets for genes encoding proteins that rely on the endoplasmic reticulum (ER) for biogenesis (Fig 1F and Dataset EV4). In contrast, GO analysis of mRNAs up-regulated by siUPF1$_{total}$ treatment yielded no significantly enriched categories. In total, 768 of the 1,621 genes up-regulated by UPF1$_{LL}$ depletion are annotated by UniProt as encoding integral membrane, secreted, and/or signal peptide-containing proteins. We also used a previous survey of ER-localized translation (Jan *et al*, 2014) to corroborate the results of the GO analysis,

finding that many $UPF1_{LL}$ target mRNAs were indeed found to be preferentially translated at the ER (Fig EV1G).

Affinity purification reveals transcriptome-wide $UPF1_{SL}$ and $UPF1_{LL}$ binding profiles

The observation that specific depletion of $UPF1_{LL}$ affected a select subpopulation of NMD targets indicated it has distinct cellular functions from those of the major $UPF1_{SL}$ isoform. To gain insight into how the biochemical properties of the two UPF1 isoforms differ, we performed affinity purification followed by RNA-seq (RIP-seq) of each UPF1 variant (Fig 2A). For these studies, we engineered HEK-293 stable cell lines to inducibly express CLIP-tagged $UPF1_{LL}$ or $UPF1_{SL}$, with a GFP-expressing stable line as a control, a system that leads to 5- to 6-fold overexpression relative to endogenous $UPF1_{total}$ levels (Fig EV2A). We elected to express CLIP-tagged UPF1 constructs, as the CLIP tag can be covalently biotinylated for efficient isolation by streptavidin affinity purification (Gautier *et al*, 2008). We have previously used this system to show that biotinylated CLIP-$UPF1_{SL}$ isolated from human cells preferentially associates with NMD-susceptible mRNA isoforms (Kishor *et al*, 2020). Analysis of well-characterized NMD substrate levels following knockdown of total endogenous UPF1 and rescue with the siRNA-resistant CLIP-UPF1 constructs confirmed that both CLIP-tagged UPF1 isoforms were equally able to function in NMD (Fig EV2B).

CLIP-UPF1 complexes were isolated from whole cell extracts by streptavidin affinity purification using a CLIP-biotin substrate, with GFP-expressing cell lines as a negative control for interaction specificity (Appendix Fig S2A). Bound RNAs were then extracted and used for sequencing library preparation. Because recovery of RNA from GFP samples was at least 100-fold lower than from CLIP-UPF1 affinity purifications (Dataset EV5), only UPF1 samples were analyzed by RNA-seq. UPF1 occupancy was assessed by normalizing the abundance of transcripts in RIP-seq samples to their abundance in total RNA-seq (hereafter referred to as UPF1 RIP-seq efficiency).

The $UPF1_{SL}$ and $UPF1_{LL}$ isoforms differ only in the domain 1B regulatory loop and therefore share a common RNA binding interface composed of residues from the RecA, 1B, 1C, and stalk domains (Chakrabarti *et al*, 2011). The majority of UPF1-RNA contacts involve sugar-phosphate recognition, enabling high-affinity, sequence-nonspecific RNA binding. Consistent with these structural features, CLIP-$UPF1_{SL}$ and CLIP-$UPF1_{LL}$ exhibited equivalent binding to the vast majority of endogenous mRNAs (mRNAs from 9711 of 10,673 genes were recovered within $\pm$ 1.4-fold in the two conditions; Fig 2B and Dataset EV5).

$UPF1_{LL}$ preferentially associates with long 3'UTRs

UPF1 accumulates in a length-dependent manner on 3'UTRs due to its active displacement from coding regions by translating ribosomes and its nonspecific RNA binding activity (Hogg & Goff, 2010; Hurt *et al*, 2013; Zünd *et al*, 2013; Kurosaki *et al*, 2014; Baker & Hogg, 2017). To evaluate the relationship between 3'UTR length and CLIP-UPF1 binding, we determined the distribution of RIP-sequencing efficiencies in three 3'UTR length bins (first tertile: < 566 nt; second tertile: 566–1,686 nt; third tertile: > 1,686 nt). Consistent with previous findings, the efficiency of mRNA co-purification with both $UPF1_{SL}$ and $UPF1_{LL}$ increased with 3'UTR length (Fig 2C).

A potential caveat to the RIP-seq studies is that the CLIP-tagged UPF1 proteins are ~5 to 6-fold overexpressed relative to endogenous $UPF1_{total}$ (Fig EV2A), which may impair the assay's discriminative power between the two isoforms. In line with this idea, binding of CLIP-$UPF1_{LL}$ and CLIP-$UPF1_{SL}$ to mRNAs from genes induced upon si$UPF1_{LL}$ and si$UPF1_{total}$ treatment was equivalent in these assays (Fig EV2C). However, one class of transcript, those with long 3'UTRs, was more efficiently co-purified with CLIP-$UPF1_{LL}$ than CLIP-$UPF1_{SL}$ (Fig 2B and C). We therefore asked whether this preferential enrichment may give clues to distinct biochemical properties of the two isoforms.

Enhanced $UPF1_{LL}$ binding to NMD-resistant transcripts

Transcripts with long 3'UTRs represent a large population of potential NMD targets (Yepiskoposyan *et al*, 2011; Hurt *et al*, 2013), only some of which are degraded by the pathway under normal conditions (Toma *et al*, 2015). Providing a biochemical mechanism to explain evasion of long 3'UTRs from decay, we have identified hundreds to thousands of mRNAs shielded by the protective RNA-binding proteins (RBPs) PTBP1 and hnRNP L (Ge *et al*, 2016; Kishor *et al*, 2019b, 2020). In our previous work, we showed that increased PTBP1 and/or hnRNP L motif binding density within the 3'UTR correlates with reduced $UPF1_{SL}$ binding and recovery of mRNAs in $UPF1_{SL}$ RIP-seq studies (Ge *et al*, 2016; Kishor *et al*, 2019b; Fritz *et al*, 2020). Based on the observation that $UPF1_{LL}$ more efficiently recovers the longest class of 3'UTRs, we asked whether mRNAs protected by PTBP1 and/or hnRNP L are differentially associated with $UPF1_{LL}$ versus $UPF1_{SL}$.

Subdivision of the transcriptome first by 3'UTR length and then according to the density of PTBP1 and hnRNP L binding sites within the 3'UTR revealed that transcripts with long 3'UTRs and moderate or high densities of protective protein binding sites were more efficiently recovered by CLIP-$UPF1_{LL}$ than CLIP-$UPF1_{SL}$ (Fig 2D and Appendix Fig S2B). This preferential recovery of long 3'UTRs with moderate or high densities of protective protein binding by CLIP-$UPF1_{LL}$ was similarly observed when PTBP1 and/or hnRNP L motif densities were restricted to the first 400 nt of the 3'UTR (Appendix Fig S2C), which we previously established as a strong feature driving protection and reduced $UPF1_{SL}$ binding (Ge *et al*, 2016; Kishor *et al*, 2019b). Quantitative RT–PCR of select transcripts confirmed these transcriptome-wide RIP-seq results (Fig EV2D and Dataset EV3).

If $UPF1_{LL}$ can more efficiently associate with mRNAs normally shielded from NMD by the protective RBPs, then we would expect a correlation between the transcripts affected by protective protein depletion and those enriched for $UPF1_{LL}$ binding. Indeed, mRNAs preferentially recovered by CLIP-$UPF1_{LL}$ were significantly downregulated in response to PTBP1 depletion in HEK-293 cells from our previous work (Ge *et al*, 2016; Data ref: Ge *et al*, 2016), a result expected for NMD substrates normally shielded by the protective RBP (Appendix Fig S2D). We observed a similar downregulation of mRNAs enriched for CLIP-$UPF1_{LL}$ binding in a publicly available RNA-seq dataset of mouse neuronal progenitor cells depleted of PTBP1 and its brain-specific paralogue PTBP2 (Appendix Fig S2E; Linares *et al*, 2015; Data ref: Linares *et al*, 2015). Together, our findings indicate that the distinct biochemical properties of $UPF1_{LL}$ give it the capacity to circumvent PTBP1 and/or hnRNP L to associate with otherwise protected mRNAs.

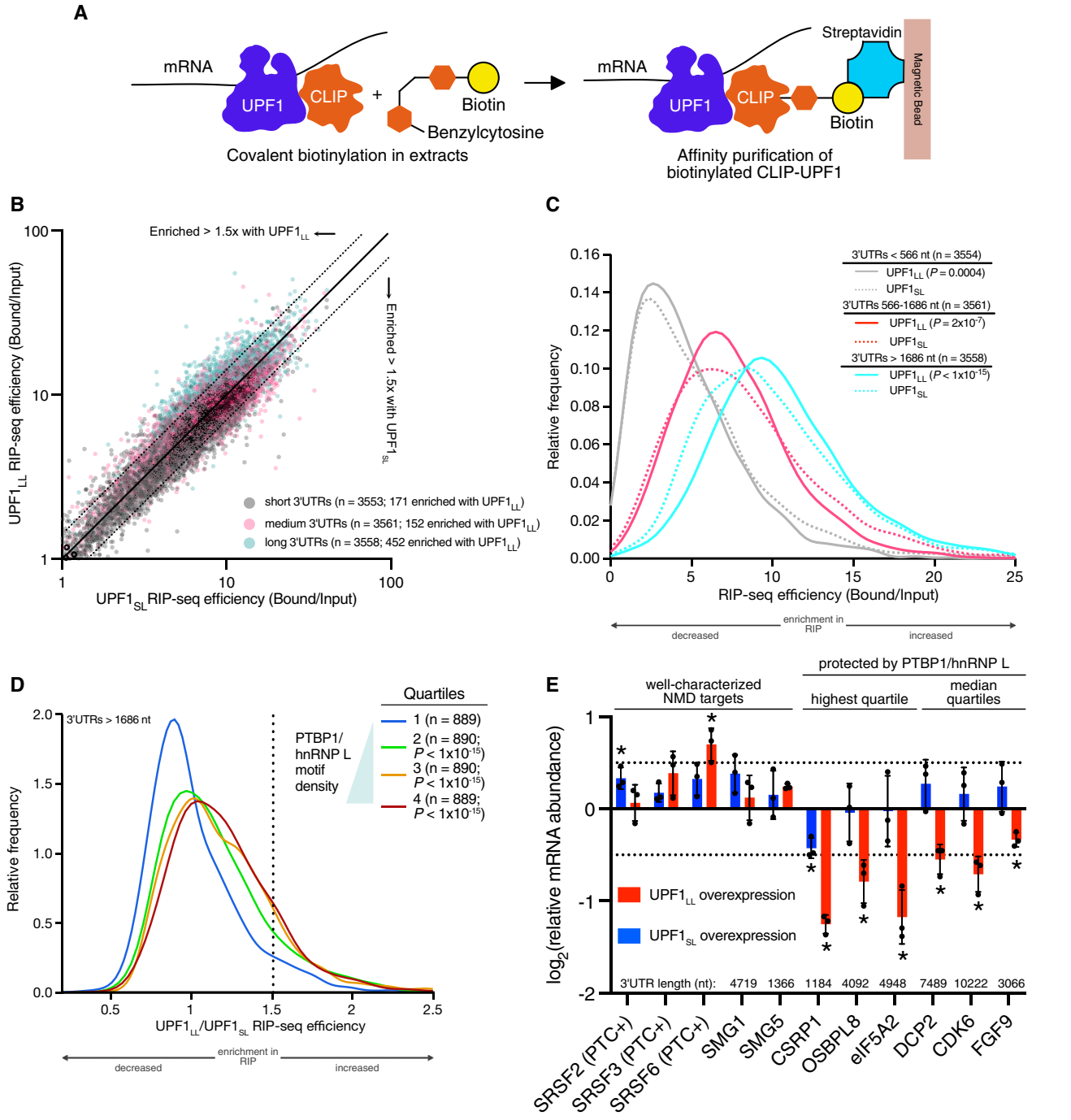

Figure 2. $UPF1_{LL}$ is enriched on NMD-protected transcripts.

A Scheme for the CLIP-UPF1 affinity purification (RIP) assay.

B Scatterplot of CLIP-$UPF1_{LL}$ vs. CLIP-$UPF1_{SL}$ RIP-seq efficiency. mRNAs were binned according to 3'UTR length (short, medium, or long).

C Density plot of recovered mRNAs in CLIP-$UPF1_{LL}$ or CLIP-$UPF1_{SL}$ affinity purifications. mRNAs were binned according to 3'UTR length. Statistical significance was determined by K–S test.

D Density plot of recovered mRNAs in CLIP-$UPF1_{LL}$ affinity purifications relative to that of CLIP-$UPF1_{SL}$. mRNAs were subdivided by PTBP1 and/or hnRNP L motif density within the 3'UTR, as indicated by the gradient triangle. Statistical significance was determined by K–W test, with Dunn's correction for multiple comparisons.

E RT–qPCR analysis of indicated transcripts from CLIP-UPF1 overexpression RNA-seq experiments. Relative fold changes are in reference to the GFP-expressing control line. Significance of CLIP-$UPF1_{SL}$ or CLIP-$UPF1_{LL}$ overexpression was compared to the GFP-expressing control line. Asterisk (*) indicates $P < 0.05$, as determined by two-way ANOVA. Black dots represent individual data points and error bars indicate mean±SD ($n = 3$ biological replicates). Dashed lines indicate $\log_2$ (fold change) of ± 0.5. For protected mRNAs, the motif density of PTBP1/hnRNP L within the 3'UTR is indicated. PTC^+ indicates the use of primers specific to transcript isoforms with validated poison exons (Lareau *et al*, 2007; Ni *et al*, 2007). See also Dataset EV3 for *P* values associated with each statistical comparison.

Source data are available online for this figure.

UPF1$_{LL}$ overexpression down-regulates mRNAs normally protected from NMD

We further analyzed the RNA-seq data from RIP-seq input samples to ask whether differential transcript recognition by the UPF1 isoforms was reflected in differential regulation upon CLIP-UPF1$_{SL}$ or CLIP-UPF1$_{LL}$ overexpression. mRNAs preferentially bound by CLIP-UPF1$_{LL}$ were systematically down-regulated upon CLIP-UPF1$_{LL}$ overexpression, but not CLIP-UPF1$_{SL}$ overexpression (Fig EV2E, top). Conversely, a small population of mRNAs preferentially recovered by CLIP-UPF1$_{SL}$ were down-regulated by CLIP-UPF1$_{SL}$ but not CLIP-UPF1$_{LL}$ overexpression (Fig EV2E, bottom). To investigate whether the observed changes in mRNA abundance with UPF1 overexpression were due to enhanced decay, we again used REMBRANDTS software (Alkallas *et al*, 2017). These analyses found that regulation of gene expression upon UPF1 overexpression was attributable to decreased mRNA stability (Fig EV2F and Dataset EV5).

We additionally corroborated the transcriptome-wide results obtained using RNA-seq by performing RT–qPCR on select transcripts (Fig 2E and Dataset EV3). Notably, validated mRNAs down-regulated by UPF1$_{LL}$ overexpression include CSRP1, which we have previously established as a long 3'UTR-containing mRNA that undergoes decay upon hnRNP L knockdown or mutation of hnRNP L binding sites in its 3'UTR (Kishor *et al*, 2019b). Reduced exogenous expression of CLIP-UPF1$_{LL}$ to levels ~0.7-fold that of total endogenous UPF1 (Appendix Fig S3A) had only small effects on levels of protected mRNAs (Appendix Fig S3B), indicating that removal of protection requires a more substantial perturbation of UPF1$_{LL}$ expression. Together, these data support the conclusion that the UPF1$_{LL}$ isoform is biochemically equipped to overcome the protective proteins to promote decay of mRNAs normally shielded from NMD, but that in cells with normal endogenous UPF1$_{SL}$ levels, protection is maintained unless UPF1$_{LL}$ is substantially overexpressed.

SRSF1 is required for expression of the UPF1$_{LL}$ splice isoform

Knockdown and overexpression of UPF1$_{LL}$ involve drastic changes in UPF1$_{LL}$ abundance, both in absolute terms and relative to UPF1$_{SL}$. We reasoned that manipulation of a regulator of UPF1 alternative splicing might allow us to manipulate the UPF1$_{LL}$:UPF1$_{SL}$ ratio without changing the total cellular UPF1 expression level. We surveyed publicly available alternative splicing analysis from ENCODE RBP knockdown RNA-seq data, which reported reduced UPF1$_{LL}$ splice isoform selection upon knockdown of the serine/arginine-rich splicing factor 1 (SRSF1) in K562 and HepG2 cells (Yee *et al*, 2019; Van Nostrand *et al*, 2020). Consistent with ENCODE data, we observed substantial and specific loss of the UPF1$_{LL}$ mRNA isoform in semi-quantitative RT–PCR assays from HEK-293 cells treated with SRSF1 siRNAs (Fig 3A). To test the functional effects of SRSF1-mediated UPF1 splicing regulation, we depleted SRSF1 from cells overexpressing CLIP-UPF1$_{SL}$ or CLIP-UPF1$_{LL}$. We chose to focus on CSRP1 mRNAs for these experiments because we have extensively validated the role of hnRNP L in antagonizing NMD of these transcripts (Kishor *et al*, 2019b) and, in this study, have shown that they are down-regulated by CLIP-UPF1$_{LL}$ overexpression (Fig 2E). Knockdown of SRSF1 caused increased CSRP1 mRNA expression, an effect that was reversed by overexpression of CLIP-UPF1$_{LL}$ but not CLIP-UPF1$_{SL}$ (Fig 3B and Dataset EV3).

We next asked whether SRSF1 overexpression would enhance use of the UPF1$_{LL}$ isoform and, if so, whether an elevated UPF1$_{LL}$:UPF1$_{SL}$ ratio would affect transcripts we have identified as responsive to UPF1$_{LL}$ knockdown or overexpression. We analyzed a public RNA-seq dataset from cells in which SRSF1 was overexpressed (Data ref: Caputi *et al*, 2019), finding an ~1.6-fold increase in usage of the UPF1$_{LL}$ mRNA isoform in SRSF1 overexpression relative to vector control cells (SRSF1 overexpression Ψ = 27.8%; vector control Ψ = 17.7%; Appendix Fig S4). This increase in UPF1$_{LL}$:UPF1$_{SL}$ ratio was associated with decreased expression of mRNAs identified as up-regulated in our siUPF1$_{LL}$ RNA-seq dataset, while the expression of mRNAs up-regulated by only siUPF1$_{total}$ was decreased (Fig 3C). Correspondingly, mRNAs preferentially bound by CLIP-UPF1$_{LL}$ versus CLIP-UPF1$_{SL}$ were systematically down-regulated by SRSF1 overexpression (Fig 3D). Together, these data establish SRSF1 as a regulator of UPF1 alternative splicing. Moreover, they indicate that relatively subtle changes in UPF1$_{LL}$:UPF1$_{SL}$ isoform ratio are sufficient to significantly favor or impair UPF1$_{LL}$ activities in cells.

UPF1$_{LL}$ is less sensitive to PTBP1-mediated inhibition of translocation

We have proposed that the protective RBPs PTBP1 and hnRNP L exploit the tendency of UPF1 to release RNA upon ATP binding and hydrolysis to promote UPF1 dissociation from potential NMD substrates prior to decay induction (Fritz *et al*, 2020). In support of this model, deletion of the regulatory loop, which mediates ATPase-dependent dissociation, rendered UPF1$_{SL}$ less sensitive to PTBP1 inhibition *in vitro* (Fritz *et al*, 2020). Importantly, both the physiological UPF1$_{LL}$ isoform and the engineered UPF1 variant containing a regulatory loop deletion exhibit a greater affinity for RNA in the presence of ATP than the PTBP1-sensitive UPF1$_{SL}$ isoform (Gowravaram *et al*, 2018). We therefore hypothesized that UPF1$_{LL}$ can mimic the ability of the loop truncation mutant to overcome negative regulation by PTBP1.

We recently established a real-time assay to monitor UPF1 translocation activity (Fritz *et al*, 2020). In this assay, UPF1 translocation and duplex unwinding causes a fluorescently labeled oligonucleotide to be displaced from the assay substrate (Fig 4A, left). An excess of complementary oligonucleotide labeled with a dark quencher is provided in the reaction, causing a decrease in fluorescence with increased displacement of the labeled oligonucleotide by UPF1. Inhibition of UPF1 translocation results in sustained fluorescence over time, allowing for the determination of inhibitory effects of PTBP1 on UPF1 unwinding activity. Using this assay in our previous work, we obtained evidence that PTBP1 inhibits UPF1 translocation rather than initial binding (Fritz *et al*, 2020). This inhibitory effect on UPF1 translocation activity was specific to PTBP1 and was not observed in the presence of the high-affinity RNA binding *Pseudomonas* phage 7 coat protein, supporting the conclusions that the protective proteins specifically promote the dissociation of UPF1 and that our assay can robustly assess inhibitors of UPF1 unwinding activity.

We therefore leveraged this system to compare UPF1$_{LL}$ versus UPF1$_{SL}$ translocation on a duplexed RNA substrate harboring a high-affinity PTBP1 binding site (Fig 4A, right) (Fritz *et al*, 2020). For these experiments, we compared the activity of highly purified UPF1 proteins containing the helicase core but lacking the

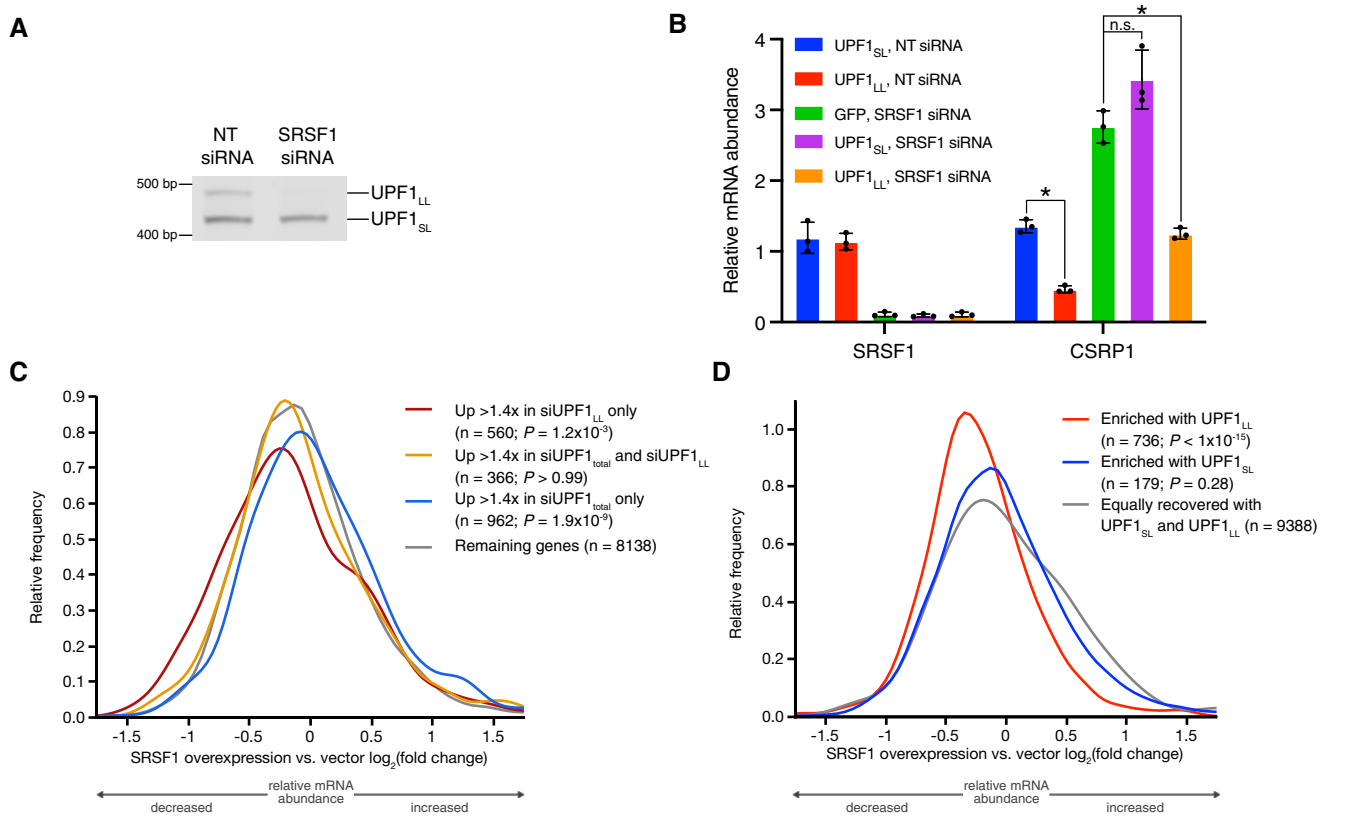

Figure 3. Splicing regulator SRSF1 is required for $UPF1_{LL}$ expression.

A Semiquantitative RT–PCR of $UPF1_{SL}$ or $UPF1_{LL}$ transcript levels following transfection of HEK-293 cells with the indicated siRNAs.

B RT–qPCR analysis of indicated transcripts following transfection of a NT siRNA or SRSF1-specific siRNA under conditions of CLIP-$UPF1_{SL}$ or CLIP-$UPF1_{LL}$ overexpression. Relative fold changes are in reference to the GFP-expressing control line treated with a NT siRNA. Asterisk (*) indicates $P < 0.05$, as determined by unpaired Student's *t*-test. Black dots represent individual data points and error bars indicate mean ± SD ($n = 3$ biological replicates). See also Dataset EV3 for *P* values associated with each statistical comparison.

C Density plot of changes in relative mRNA abundance as determined by RNA-seq following SRSF1 overexpression (Data ref: Caputi *et al*, 2019). Genes were categorized as up-regulated by $siUPF1_{total}$ only, $siUPF1_{LL}$ only, or both $siUPF1_{total}$ and $siUPF1_{LL}$. Statistical significance was determined by K–W test, with Dunn's correction for multiple comparisons.

D Density plot as in (C), with genes binned according to enrichment in the CLIP-$UPF1_{LL}$ or CLIP-$UPF1_{SL}$ affinity purifications.

Source data are available online for this figure.

autoinhibitory N-terminal cysteine-histidine domain (UPF1ΔCH) (Appendix Fig S5A and B; Chakrabarti *et al*, 2011; Fiorini *et al*, 2012; Fritz *et al*, 2020). $UPF1_{SL}$ΔCH exhibited robust unwinding activity in the absence of PTBP1, displacing 50% of the duplexed oligonucleotide in 100 s (Fig 4B). This translocation activity of $UPF1_{SL}$ΔCH was dependent upon the addition of ATP, as previously demonstrated (Fritz *et al*, 2020). Addition of PTBP1 substantially impaired $UPF1_{SL}$ΔCH unwinding activity, reducing both the rate at which the oligonucleotide was displaced (requiring 360 s to attain the half-maximal unwinding value reached by $UPF1_{SL}$ΔCH alone) and the overall extent of unwinding (73% of the $UPF1_{SL}$ΔCH total at the end of the assay).

$UPF1_{LL}$ΔCH also exhibited robust unwinding activity in the absence of PTBP1, displacing 50% of the duplexed oligonucleotide in 90 s in an ATP-dependent manner (Fig 4C). The observed enhancement in $UPF1_{LL}$ΔCH translocation activity over $UPF1_{SL}$ΔCH is consistent with previous reports of increased catalytic activity of the $UPF1_{LL}$ isoform relative to $UPF1_{SL}$ (Gowravaram *et al*, 2018). In contrast to $UPF1_{SL}$ΔCH, $UPF1_{LL}$ΔCH maintained robust unwinding activity in the presence of PTBP1, displacing 50% of the duplexed oligonucleotide by 180 s and achieving 94% total duplex unwinding at the end of the assay. These results indicate that $UPF1_{LL}$ can overcome the translocation inhibition by PTBP1, reinforcing the conclusion that PTBP1-mediated UPF1 inhibition depends on the clash between the UPF1 regulatory loop and RNA.

Coordinated downregulation of $UPF1_{LL}$ targets during ER stress and ISR induction

Our *in vitro*, RIP-seq, and overexpression studies suggested that $UPF1_{LL}$ has the biochemical capacity to expand the scope of UPF1-dependent regulation. Based on these observations, we next investigated whether specific physiological conditions might promote changes in NMD target susceptibility by harnessing endogenous $UPF1_{LL}$ activity. Multiple lines of evidence led us to examine the regulation of $UPF1_{LL}$ in the integrated stress response (ISR),

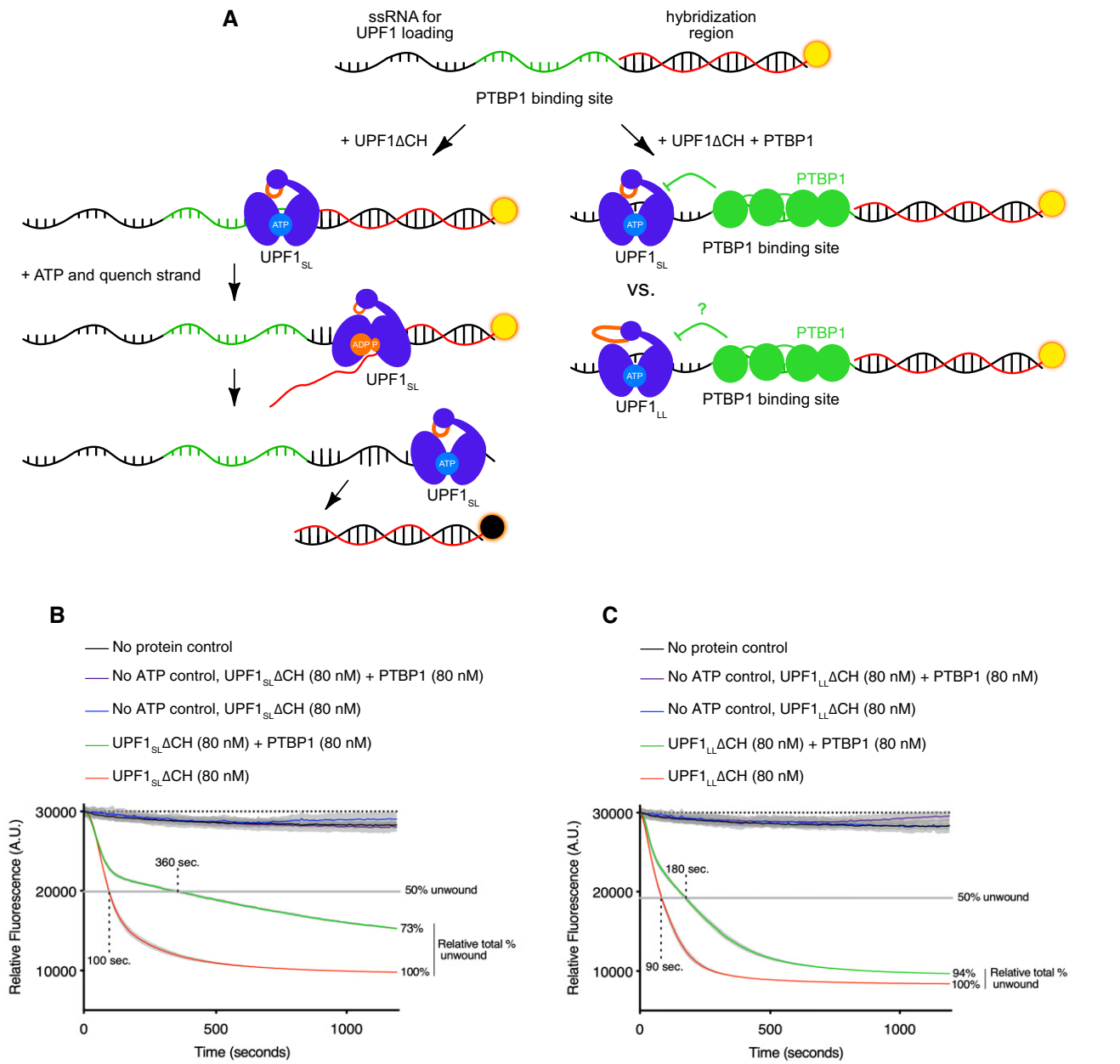

Figure 4. UPF1$_{LL}$ overcomes translocation inhibition by PTBP1.

A Scheme of the fluorescence-based unwinding assay to monitor UPF1 translocation in real-time (Fritz *et al*, 2020). An RNA substrate harboring a high-affinity PTBP1 binding site is incubated with highly purified UPF1ΔCH in the absence and presence of equal molar amounts of highly purified PTBP1. Upon the addition of ATP, UPF1 translocation results in a decrease in fluorescence due to displacement of a labeled, duplexed oligonucleotide and subsequent quenching by a trap strand.

B UPF1$_{SL}$ΔCH translocation along an RNA substrate harboring a high-affinity PTBP1 binding site in the absence and presence of PTBP1. Time to 50% unwound and relative total % unwound at end of assay (1,200 s) are indicated. Results of four technical replicates are shown for each dataset and represent at least three independent experiments. Shaded region indicates SD.

C Results as in (B) but with UPF1$_{LL}$ΔCH.

Source data are available online for this figure.

which restores homeostasis by repressing translation and inducing expression of a battery of stress response genes (Fig 5A; Costa-Mattioli & Walter, 2020). Activation of the ISR induces hyperphosphorylation of eIF2α, driving global downregulation of protein synthesis due to impaired eIF2-GTP-Met-tRNA$_i$ ternary complex recycling and reduced delivery of the initiator Met-tRNA$_i$ to translating ribosomes (Baird & Wek, 2012; Young & Wek, 2016; Wek, 2018). An established effect of ISR-mediated translational repression is corresponding stabilization of well-characterized NMD targets, including several mRNAs encoding factors integral to the

activation and resolution of the stress response (Goetz & Wilkinson, 2017).

Two of our findings led us to consider the possibility that $UPF1_{LL}$ activity is regulated by the ISR. First, GO analyses indicated substantial enrichment of ER-localized mRNAs among those up-regulated by $UPF1_{LL}$ knockdown (Fig 1F). Second, as an initial test of the hypothesis that certain cellular conditions would promote turnover of mRNAs preferentially bound by CLIP-$UPF1_{LL}$, we analyzed a published RNA-seq dataset from cells treated with the ISR-inducing agent tunicamycin (Park *et al*, 2017; Data ref: Park *et al*, 2017). This analysis identified systematic downregulation of mRNAs enriched in CLIP-$UPF1_{LL}$ RIP-seq, in contrast to RNAs preferentially bound by CLIP-$UPF1_{SL}$ (Fig EV3A).

We next directly assessed how $UPF1_{LL}$ activity contributes to gene expression regulation during ER stress and induction of the ISR by performing RNA-seq of HEK-293 cells treated with the ER stress-inducing agent thapsigargin (Fig 5B and Dataset EV6). Western blot analysis showed a 2.5-fold increase in eIF2α phosphorylation with thapsigargin treatment (Fig EV3B), supporting a robust induction of the ISR. Consistent with previous results (Nickless *et al*, 2014; Li *et al*, 2017), mRNAs up-regulated upon total UPF1 knockdown in HEK-293 cells were on average also up-regulated following 6 or 9 h in 1 μM thapsigargin (Fig 5B), and the magnitude of the increase correlated with the effects of UPF1 total knockdown. In sharp contrast, genes up-regulated by $UPF1_{LL}$-specific knockdown exhibited a distinct behavior upon thapsigargin treatment. Rather than increasing, $UPF1_{LL}$ substrates showed on average a reduction in mRNA levels, and this tendency did not vary according to the magnitude of the effect of $UPF1_{LL}$ knockdown. These results indicate that $UPF1_{LL}$ functions distinctly from that of well-characterized NMD and sustains activity during ER stress and activation of the ISR.

$UPF1_{LL}$ conditionally remodels NMD target selection during ER stress and ISR induction

To more comprehensively evaluate the role of $UPF1_{LL}$ in promoting the downregulation of select genes during ISR induction, we transfected HEK-293 cells with non-targeting (NT) or $UPF1_{LL}$-specific siRNAs and then treated cells with 1 μM thapsigargin for 6 or 9 h (Fig EV3C). In RNA-seq analyses, we identified 606 genes that significantly decreased in abundance with thapsigargin treatment, of which 135 (6 h) or 143 (9 h) were rescued at least 1.4-fold upon $UPF1_{LL}$ knockdown (Fig 5C, Appendix Fig S6A, and Dataset EV6). In contrast, only 70 (6 h) or 62 (9 h) of these 606 genes decreased in abundance in response to $UPF1_{LL}$ knockdown in thapsigargin treatment. These results were highly reproducible between the 6 h and 9 h thapsigargin RNA-seq datasets (Appendix Fig S6B), supporting that a unique population of genes are selectively down-regulated during conditions of ER stress and induction of the ISR in a $UPF1_{LL}$-dependent manner.

Inferred mRNA stability changes using REMBRANDTS software supported that the observed differences in mRNA abundance upon thapsigargin treatment and $UPF1_{LL}$ knockdown were due to changes in mRNA decay (Fig EV3D and E). The changes in gene expression caused by $UPF1_{LL}$ depletion were not attributable to differential ISR induction, as previously established stress response genes were comparably up-regulated in response to thapsigargin treatment following NT and $UPF1_{LL}$-specific knockdown (Fig EV3F; Ashburner *et al*, 2000; The Gene Ontology Consortium, 2019). Moreover, thapsigargin treatment did not alter the relative levels of $UPF1_{LL}$ and $UPF1_{SL}$ mRNAs (Fig EV3G), indicating that $UPF1_{LL}$ activity in ER stress was likely due to activity of the existing population of protein rather than a consequence of altered UPF1 splicing upon thapsigargin treatment.

Our finding that $UPF1_{LL}$ has the potential to bind and regulate transcripts protected from NMD by PTBP1 and/or hnRNP L under normal cell growth conditions (Figs 2 and EV2) led us to ask whether genes down-regulated by $UPF1_{LL}$ during ISR induction included substrates beyond those identified as $UPF1_{LL}$ targets under normal cellular conditions (Fig 1). Of the 135 genes down-regulated by $UPF1_{LL}$ upon thapsigargin treatment, 49 genes (36%) were unique to the population of $UPF1_{LL}$ targets down-regulated during ISR induction, while 86 genes were identified as $UPF1_{LL}$ targets under both normal and stress conditions (Fig 5C). These data indicate that $UPF1_{LL}$ activity is maintained or enhanced when cells are subjected to ER stress conditions that inhibit well-characterized NMD events.

To corroborate the above findings, we performed RT–qPCR on select transcripts identified by RNA-seq as constitutively or conditionally regulated by $UPF1_{LL}$ (Fig 5D and Dataset EV3). As in the RNA-seq analyses, RT–qPCR of putative condition-specific $UPF1_{LL}$ targets revealed several mRNAs (e.g., TMEM165, LDLR, TIMP2, NXT2, TGOLN2, and COL4A1) that exhibited $UPF1_{LL}$-dependent downregulation upon thapsigargin treatment but were not affected by $siUPF1_{LL}$ under normal growth conditions. Taken together, these data support a model in which expression of dual $UPF1_{SL}$ and $UPF1_{LL}$ isoforms enable conditional remodeling of NMD target selection in response to ISR induction.

Figure 5. $UPF1_{LL}$ conditionally remodels NMD target selection during ER stress and induction of the ISR.

A Scheme for activation of the integrated stress response (ISR) and effects on UPF1-dependent decay.

B Density plots of changes in relative mRNA abundance as determined by RNA-seq following treatment of HEK-293 cells with 1 μM thapsigargin for 6 h (left) or 9 h (right). Genes were categorized as up-regulated by $siUPF1_{total}$ only or $siUPF1_{LL}$ only under basal conditions. Statistical significance was determined by K–W test, with Dunn's correction for multiple comparisons.

C RNA-seq analysis of HEK-293 cells identifies populations of genes that decreased in abundance with thapsigargin treatment and were rescued by $UPF1_{LL}$-specific knockdown. Indicated are genes that increased in abundance at least 1.4-fold (FDR < 0.05) with $UPF1_{LL}$-specific knockdown under normal conditions.

D RT–qPCR analysis of indicated transcripts following transfection of HEK-293 cells with indicated siRNAs and treatment with 1 μM thapsigargin for 6 h. Relative fold changes are in reference to vehicle-treated, NT siRNA. Black dots represent individual data points and error bars indicate mean ± SD (n = 3 biological replicates). Dashed lines indicate $\log_2$ (fold change) of ± 0.5. PTC^+ indicates the use of primers specific to transcript isoforms with validated poison exons (Lareau *et al*, 2007; Ni *et al*, 2007). See also Dataset EV3 for *P*-values associated with each statistical comparison.

Source data are available online for this figure.

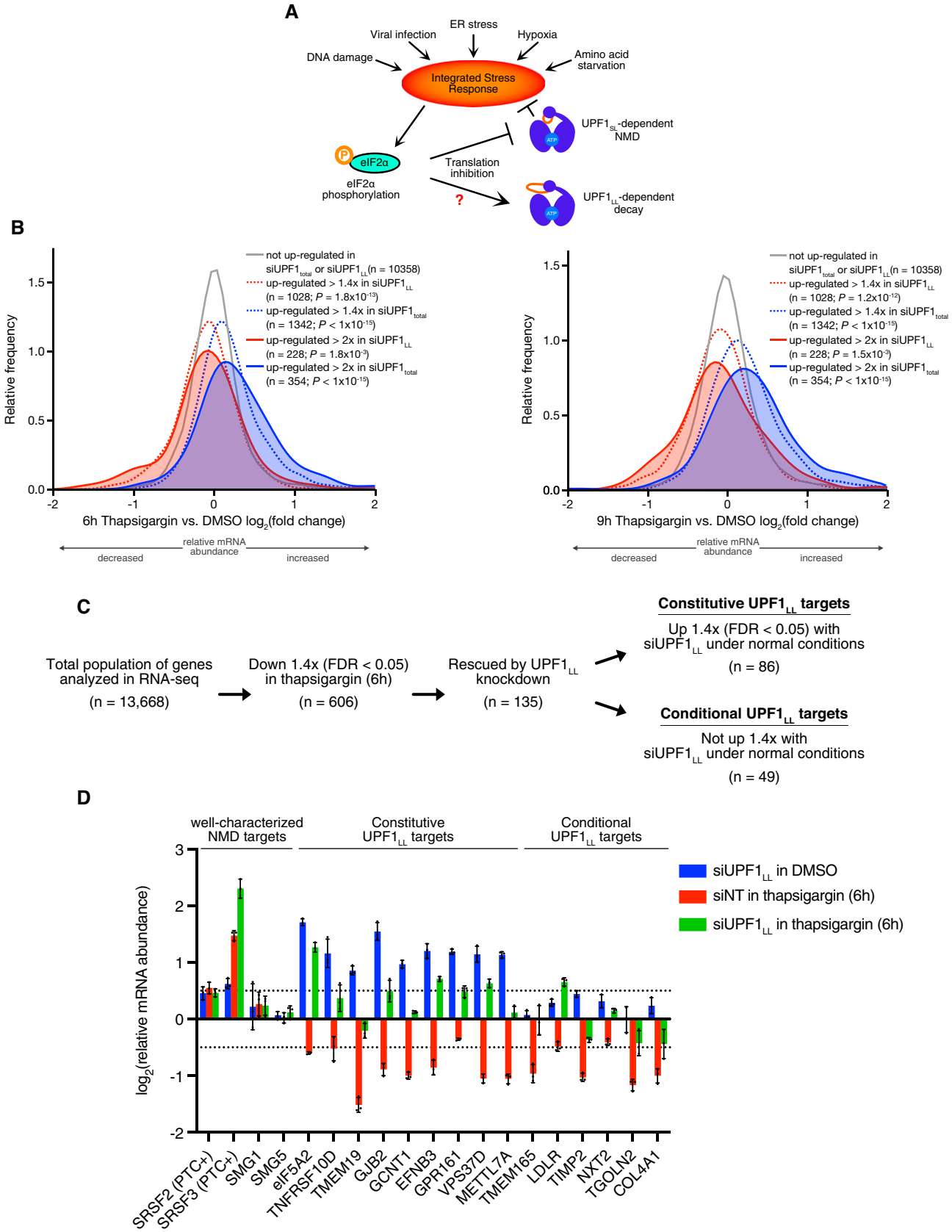
A
Viral infection
ER stress
Hypoxia
DNA damage
Amino acid starvation
Integrated Stress Response
UPF1SL-dependent NMD
eIF2α
eIF2α phosphorylation
Translation inhibition
?
UPF1LL-dependent decay
B
not up-regulated in siUPF1total or siUPF1LL(n = 10358)
up-regulated > 1.4x in siUPF1LL (n = 1028; P = 1.8x10-13)
up-regulated > 1.4x in siUPF1total (n = 1342; P < 1x10-15)
up-regulated > 2x in siUPF1LL (n = 228; P = 1.8x10-3)
up-regulated > 2x in siUPF1total (n = 354; P < 1x10-15)
Relative frequency
6h Thapsigargin vs. DMSO log2(fold change)
decreased
relative mRNA abundance
increased
not up-regulated in siUPF1total or siUPF1LL(n = 10358)
up-regulated > 1.4x in siUPF1LL (n = 1028; P = 1.2x10-12)
up-regulated > 1.4x in siUPF1total (n = 1342; P < 1x10-15)
up-regulated > 2x in siUPF1LL (n = 228; P = 1.5x10-3)
up-regulated > 2x in siUPF1total (n = 354; P < 1x10-15)
Relative frequency
9h Thapsigargin vs. DMSO log2(fold change)
decreased
relative mRNA abundance
increased
C
Total population of genes analyzed in RNA-seq
(n = 13,668)
Down 1.4x (FDR < 0.05) in thapsigargin (6h)
(n = 606)
Rescued by UPF1LL knockdown
(n = 135)
Constitutive UPF1LL targets
Up 1.4x (FDR < 0.05) with siUPF1LL under normal conditions
(n = 86)
Conditional UPF1LL targets
Not up 1.4x with siUPF1LL under normal conditions
(n = 49)
D
well-characterized NMD targets
Constitutive UPF1LL targets
Conditional UPF1LL targets
log2(relative mRNA abundance)
siUPF1LL in DMSO
siNT in thapsigargin (6h)
siUPF1LL in thapsigargin (6h)
SRSF2 (PTC+)
SRSF3 (PTC+)
SMG1
SMG5
eIF5A2
TNFRSF10D
TMEM19
GJB2
GCNT1
EFNB3
GPR161
VPS37D
METTL7A
TMEM165
LDLR
TIMP2
NXT2
TGOLN2
COL4A1

Figure 5.

$UPF1_{LL}$ target repertoire is expanded by partial translational repression

Because NMD requires detection of in-frame stop codons, target susceptibility is sensitive to changes in the location and frequency of translation initiation and termination. In addition to modulation of initiation via eIF2α phosphorylation in ER stress (Goetz & Wilkinson, 2017), inhibition of translation elongation (e.g., with cycloheximide and puromycin) inhibits the decay of well-characterized NMD targets (Carter *et al*, 1995). We therefore asked whether translational repression would promote $UPF1_{LL}$ activity outside of the context of the ISR (Fig 6A).

We again compared published RNA-seq datasets with our UPF1 RIP-seq data to provide a preliminary test of this hypothesis. As we observed using published RNA-seq data from cells undergoing ER stress, mRNAs preferentially bound by $UPF1_{LL}$ were systematically down-regulated upon treatment with moderate doses of the initiation inhibitor hippuristanol or the elongation inhibitors emetine and cycloheximide (Fig EV4A–C) (Data ref: Martinez-Nunez & Sanford, 2016; Martinez-Nunez *et al*, 2017; Kearse *et al*, 2019; Data ref: Kearse *et al*, 2019; Waldron *et al*, 2019; Data ref: Waldron *et al*, 2019). In the case of cycloheximide treatment, only 15 min of treatment was sufficient to observe significant loss of $UPF1_{LL}$-enriched transcripts, consistent with a decay-driven process.

We next used $siUPF1_{LL}$ treatment to directly test whether mRNAs down-regulated upon moderate translation inhibition required $UPF1_{LL}$. We elected to use the translation elongation inhibitor puromycin for these experiments because it is widely used to inhibit canonical NMD events and acts through a completely distinct mechanism from the block to initiation caused by eIF2α phosphorylation. Specifically, the ribosome catalyzes the linkage of puromycin to nascent polypeptides, causing chain termination and peptide release (Nathans, 1964).

To investigate whether $UPF1_{LL}$ is able to exert sustained or even enhanced post-transcriptional control in response to translation inhibition via distinct mechanisms, we transfected HEK-293 cells with NT or $UPF1_{LL}$-specific siRNAs and then treated cells with puromycin (50 μg/ml for 4 h; Fig EV5A). Remarkably, RNA-seq analyses revealed 2,279 genes that significantly decreased in abundance with puromycin treatment, of which 700 (31%) were rescued at least 1.4-fold upon $UPF1_{LL}$ knockdown (Fig 6B and Dataset EV7). In contrast, only 124 genes (5%) decreased in abundance in response to $UPF1_{LL}$ knockdown in puromycin treatment (Appendix Fig S7A). The response to $UPF1_{LL}$ depletion was highly consistent in cells treated with in 25, 50, and 100 μg/ml puromycin (Appendix Fig S7B), supporting a role for $UPF1_{LL}$ in gene expression regulation during conditions of partial translational repression. Genes identified as destabilized in REMBRANDTS analysis of CLIP-$UPF1_{LL}$ versus CLIP-$UPF1_{SL}$ overexpression tended to be down-regulated upon puromycin treatment, while the reverse was true for genes preferentially destabilized by CLIP-$UPF1_{SL}$ overexpression (Fig EV5B). Consistent with a specific role for $UPF1_{LL}$, knockdown of $UPF1_{LL}$ ameliorated the effects of puromycin treatment on genes regulated by CLIP-$UPF1_{LL}$ but not CLIP-$UPF1_{SL}$ overexpression.

We next employed puromycin to identify new conditional $UPF1_{LL}$ targets, finding that 550 genes (79%) identified as rescued by $UPF1_{LL}$ from puromycin-dependent downregulation were uniquely affected during puromycin treatment. The remaining 150 genes (21%) significantly overlapped with those up-regulated with $UPF1_{LL}$ depletion under normal cellular conditions (Fig 6B). RT–qPCR of select transcripts confirmed the transcriptome-wide RNA-seq results (Fig 6C and Dataset EV3). Similar to conditions of ER stress, puromycin treatment did not alter UPF1 splicing (Fig EV5C), indicating that $UPF1_{LL}$ activity during conditions of impaired translation was likely due to the existing population of $UPF1_{LL}$ protein. These data support that translational repression promotes $UPF1_{LL}$ activity outside of the context of the ISR to conditionally remodel NMD target selection.

$UPF1_{LL}$ activity requires ongoing translation

Because of the well-established requirement for translation in NMD, we hypothesized that the UPF1 isoform-dependent effects of thapsigargin and moderate puromycin treatment were due to changes in the location and/or frequency of translation termination events (Fig 6A). To test this hypothesis, we treated cells with a titration of puromycin from 25 μg/mL to 400 μg/ml. If $UPF1_{LL}$ activity depends on the infrequent residual translation termination events that occur under puromycin treatment, its activity should be enhanced at low concentrations of puromycin that permit some termination events to persist but be inhibited by high concentrations of puromycin that more efficiently block translation.

In line with these expectations, we observed a dose-dependent response, in which downregulation of representative $UPF1_{LL}$ target transcripts FMR1, eIF5A2, ERBB2, and CDK16 was most efficient at lower puromycin concentrations (Fig EV5D and Dataset EV3). Treatment with high concentrations of puromycin did not have a significant effect on the levels of these $UPF1_{LL}$ target mRNAs, consistent with a requirement for translation termination events. Corroborating these findings, we observed globally more efficient downregulation of puromycin-sensitive $UPF1_{LL}$ targets with 25 μg/ml puromycin than 100 μg/ml puromycin in RNA-seq (Fig EV5E and Dataset EV7). Based on these results, we conclude that translation termination is likely required for all UPF1-dependent decay events but that changes in translation efficiency can drive the downregulation of a novel class of substrates by the $UPF1_{LL}$ isoform.

Translational repression promotes $UPF1_{LL}$-dependent decay of select mRNAs

Inferred mRNA stability changes using REMBRANDTS software indicated that the observed differences in mRNA abundance upon puromycin treatment and $UPF1_{LL}$ knockdown from the RNA-seq studies were due to corresponding changes in mRNA stability (Fig EV5F and G and Dataset EV7). To directly evaluate the effect of translational repression on promoting the decay of mRNAs by $UPF1_{LL}$, we leveraged the recently established method of Roadblock-qPCR to assess endogenous mRNA stability (Watson *et al*, 2021). In this method, 4-thiouridine (4-SU) is used to label transcripts produced during a 4-h timecourse. Isolated RNA is treated with N-ethylmaleimide, which covalently labels 4-SU residues, forming a bulky adduct that blocks reverse transcription. RT–qPCR of the remaining unlabeled pool thus allows straightforward quantification of mRNA turnover.

HEK-293 cells were transfected with NT or $UPF1_{LL}$-specific siRNAs and labeled with 4-SU in the absence and presence of

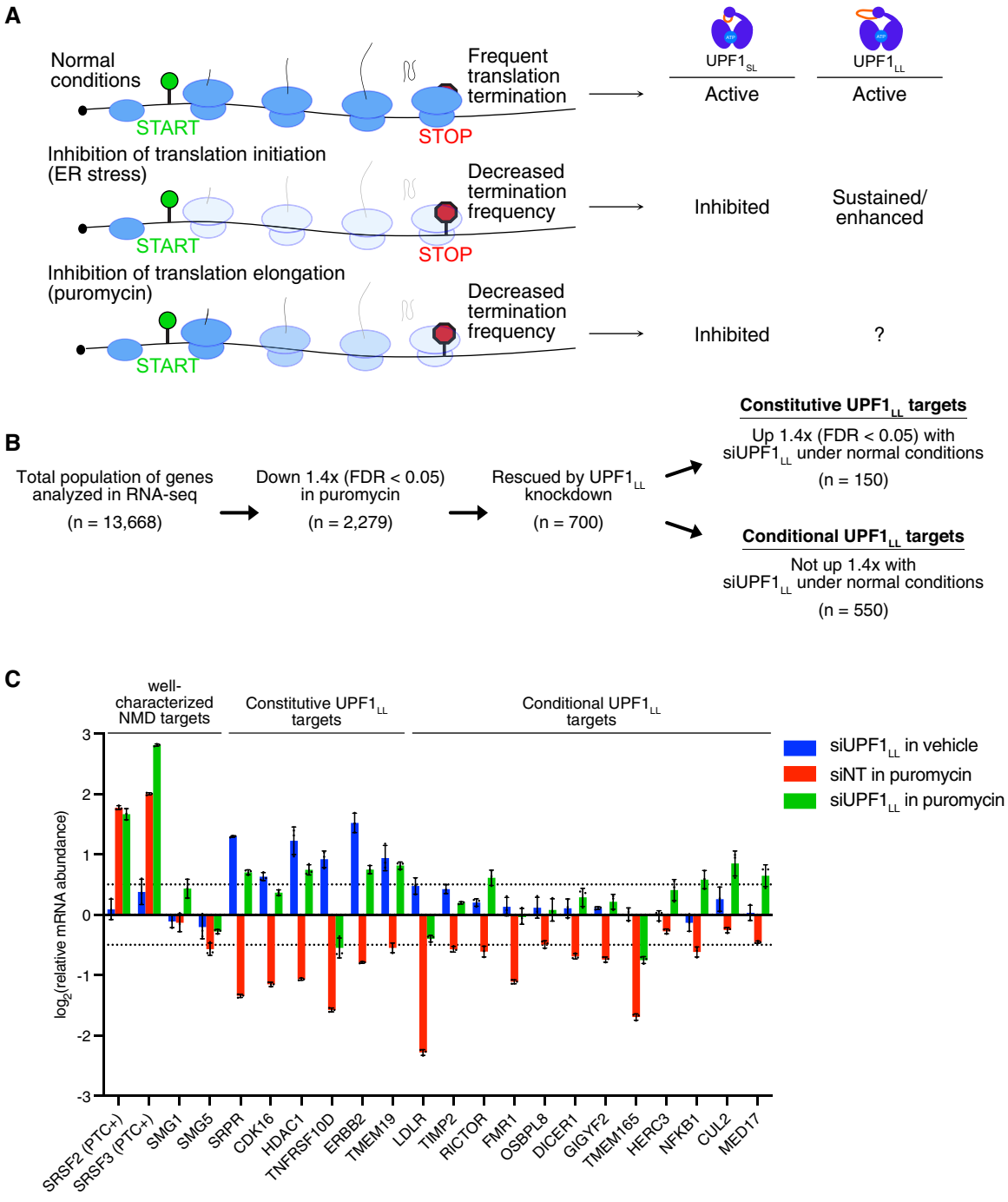

Figure 6. UPF1$_{LL}$ activity is enhanced by translational repression.

A Framework for investigation of effects of translation inhibition on UPF1$_{LL}$ activity.

B RNA-seq analysis of HEK-293 cells identifies populations of genes that decreased in abundance with puromycin treatment (50 μg/ml for 4 h) and were rescued by UPF1$_{LL}$-specific knockdown. Indicated are genes that increased in abundance at least 1.4-fold (FDR < 0.05) with UPF1$_{LL}$-specific knockdown under normal conditions.

C RT–qPCR analysis of indicated transcripts following transfection of HEK-293 cells with indicated siRNAs and treatment with 50 μg/ml puromycin for 4 h. Relative fold changes are in reference to vehicle-treated, NT siRNA. Black dots represent individual data points, and error bars indicate mean ± SD (n = 3 biological replicates). Dashed lines indicate log$_2$ (fold change) of ± 0.5. PTC$^+$ indicates the use of primers specific to transcript isoforms with validated poison exons (Lareau *et al*, 2007; Ni *et al*, 2007). See also Dataset EV3 for *P*-values associated with each statistical comparison.

Source data are available online for this figure.

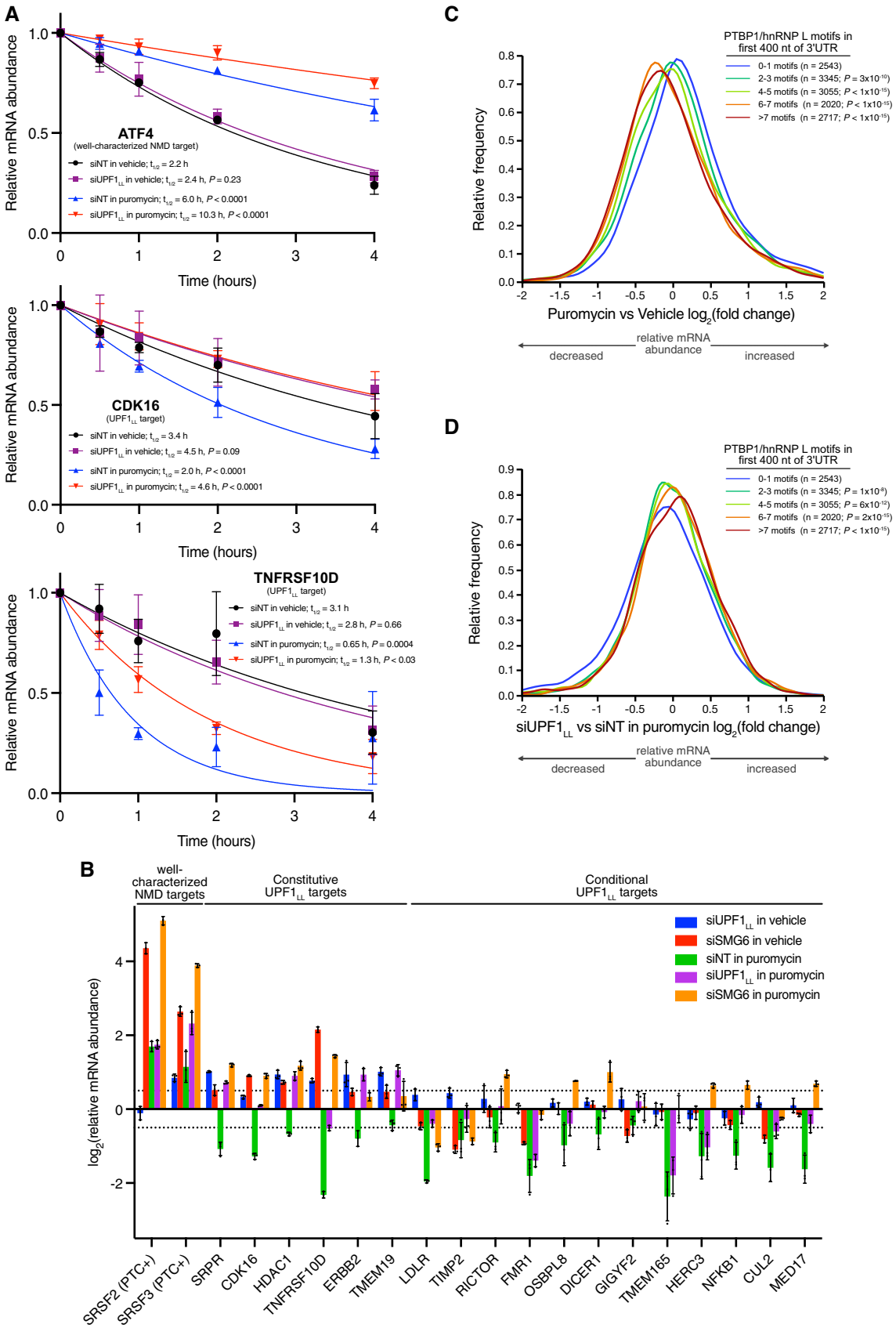

Figure 7.

Figure 7. Translational repression promotes the decay of mRNAs by UPF1$_{LL}$ in the NMD pathway and down-regulates normally protected transcripts.

A mRNA decay measurement using Roadblock-qPCR (Watson *et al*, 2021). RNA was isolated from HEK-293 cells at indicated timepoints following transfection with indicated siRNAs and treatment with 400 μM 4sU and 50 μg/ml puromycin. mRNA half-lives were estimated by fitting the data to a single-phase exponential decay model. Puromycin treatment was compared to the vehicle control and siUPF1$_{LL}$ was compared to the siNT in the absence and presence of puromycin treatment using the extra-sum-of-squares *F* test. Error bars indicate mean ± SD (n = 4 biological replicates). See also Dataset EV3 for *P* values associated with each statistical comparison.

B RT–qPCR analysis of indicated transcripts following transfection of HEK-293 cells with indicated siRNAs and treatment with 50 μg/ml puromycin for 4 h. Relative fold changes are in reference to vehicle-treated, NT siRNA. Black dots represent individual data points and error bars indicate mean ± SD (n = 3 biological replicates). Dashed lines indicate $\log_2$ (fold change) of ± 0.5. PTC$^+$ indicates the use of primers specific to transcript isoforms with validated poison exons (Lareau *et al*, 2007; Ni *et al*, 2007). See also Dataset EV3 for *P* values associated with each statistical comparison.

C Density plot of changes in relative mRNA abundance as determined from RNA-seq following treatment of HEK-293 cells with 50 μg/ml of puromycin for 4 h. mRNAs were subdivided by PTBP1 and/or hnRNP L motif density within the first 400 nt of 3'UTR. Statistical significance was determined by K–W test, with Dunn's correction for multiple comparisons.

D Density plot as in (C), following UPF1$_{LL}$-specific knockdown.

Source data are available online for this figure.

puromycin. In this analysis, puromycin treatment stabilized the canonical NMD target of ATF4 (Fig 7A and Dataset EV3), consistent with previous findings that translational repression inhibits decay of well-characterized NMD targets. In contrast, representative UPF1$_{LL}$ targets CDK16 and TNFRSF10D exhibited significantly shorter half-lives with puromycin treatment, an effect that was dependent upon UPF1$_{LL}$ expression. Together, these data support the conclusion that translational repression promotes the decay of mRNAs by UPF1$_{LL}$.

UPF1$_{LL}$ activity during translational repression requires SMG6

We next asked whether UPF1$_{LL}$-dependent mRNA downregulation during translational repression involved the specialized NMD endonuclease SMG6. To explore this possibility, HEK-293 cells were transfected with NT or SMG6-specific siRNAs and then treated with puromycin. Quantitative RT–PCR of select transcripts revealed that knockdown of SMG6 significantly rescued the downregulation of UPF1$_{LL}$ targets in puromycin treatment (Fig 7B and Dataset EV3). This effect was comparable to that observed with UPF1$_{LL}$-specific depletion, supporting the conclusion that select mRNA downregulation during translational repression is due to UPF1$_{LL}$ activity in the NMD pathway. Furthermore, knockdown of SMG6 under normal conditions increased the abundance of well-characterized NMD targets and constitutively regulated UPF1$_{LL}$ substrates but did not significantly affect the levels of conditionally regulated UPF1$_{LL}$ substrates. These results provide further evidence that UPF1$_{LL}$ remodels NMD target selection during translational repression to promote the decay of a new class of substrates.

NMD-protected mRNAs are down-regulated by UPF1$_{LL}$ during translational repression

Finally, we asked whether the expanded functions of UPF1$_{LL}$ in translational repression are related to its biochemical capability to direct degradation of mRNAs normally protected by PTBP1 and/or hnRNP L. We analyzed whether RNAs with stop codon-proximal PTBP1 and hnRNP L motifs are among those susceptible to UPF1$_{LL}$-mediated downregulation upon puromycin treatment. Subdivision of the transcriptome according to PTBP1 and/or hnRNP L motif binding density within the first 400 nt of the 3'UTR revealed that mRNAs with high densities of binding sites for the protective proteins were significantly down-regulated with puromycin treatment relative to mRNAs with low densities of binding sites (Fig 7C). Knockdown of UPF1$_{LL}$ rescued this decrease in mRNA abundance, supporting the conclusion that the downregulation of protected mRNAs during translational repression was dependent upon UPF1$_{LL}$ expression (Fig 7D). Based on these data, we conclude that enhanced UPF1$_{LL}$ activities upon translational repression result in deprotection of normally NMD-insensitive mRNAs.

Discussion

Here, we employ specific depletion, overexpression, and biochemical methods to identify that the mammalian UPF1$_{LL}$ isoform performs distinct functions from that of the major UPF1$_{SL}$ isoform. By depleting only the UPF1$_{LL}$-encoding mRNA, we show that UPF1$_{LL}$ is required for a subset of UPF1-mediated regulation, preferentially targeting mRNAs that encode transmembrane and secreted proteins translated at the ER (Fig 1). Our transcriptome-wide studies of UPF1$_{LL}$ and UPF1$_{SL}$ RNA binding reveal that UPF1$_{LL}$ has a greater capacity to bind and regulate mRNAs normally protected from decay by PTBP1 and hnRNP L (Fig 2). The endogenous expression of UPF1$_{LL}$ depends on the splicing regulator SRSF1; correspondingly, manipulation of SRSF1 levels by knockdown or overexpression causes impaired or enhanced UPF1$_{LL}$ activity, respectively (Fig 3). The cellular interaction specificity of UPF1$_{LL}$ is corroborated by its ability to overcome inhibition by PTBP1 *in vitro* (Fig 4), consistent with our previous observation that PTBP1 promotes ATPase-dependent UPF1 dissociation by exploiting the UPF1 regulatory loop (Fritz *et al*, 2020). These data in sum suggest that UPF1$_{LL}$ has the biochemical capability to regulate the protected population of mRNAs but that its activities are likely constrained by its relatively low expression in HEK-293 and many other cell types.

In contrast to the well-characterized inhibition of NMD by ER stress, we find that UPF1$_{LL}$-dependent regulation is intact or even enhanced (Fig 5). Mechanistically, preferential UPF1$_{LL}$ activity in ER stress can be explained by its ability to function under conditions of translational repression (Fig 6). Moderate inhibition of translation with puromycin causes thousands of genes to be down-regulated, of which approximately one-third are rescued by UPF1$_{LL}$ knockdown. These experiments show that UPF1$_{LL}$ is not only required for down-regulation of mRNAs identified as substrates under normal

conditions ("constitutive" $UPF1_{LL}$ targets), but also regulates additional mRNAs under ER stress and translational repression ("conditional" $UPF1_{LL}$ targets). mRNAs that are down-regulated by $UPF1_{LL}$ upon puromycin treatment are enriched for stop codon-proximal protective protein binding sites, providing a mechanism for their conditional, isoform-specific targeting (Fig 7). Combined with the inhibition of $UPF1_{SL}$-dependent decay, enhanced $UPF1_{LL}$ activity upon translational repression results in a dramatic and unanticipated shift in NMD target specificity.

We present a model in which moderate translational repression does not uniformly repress NMD but instead alters its specificity (Fig 8). In this model, the relative activity of $UPF1_{LL}$ expands as translation activity decreases, allowing continued degradation of constitutive $UPF1_{LL}$ targets and inducing downregulation of new substrate mRNAs. The change in NMD specificity upon translational repression is enabled by the distinct biochemical properties of the $UPF1_{LL}$ protein. First, $UPF1_{LL}$ has an intrinsically enhanced affinity for RNA in the presence of ATP (Gowravaram *et al*, 2018), which may allow prolonged association with mRNAs and increase the probability that UPF1 binding co-occurs with translation termination. Second, $UPF1_{LL}$ is able to overcome inhibition by protective proteins such as PTBP1, which allows targeting of mRNAs normally shielded from decay (Fig 2).

We envision that the two UPF1 isoforms may compete for less abundant NMD factors, particularly under conditions that impair decay or translation. An attractive possibility is that persistent binding of $UPF1_{LL}$ to mRNAs promotes its phosphorylation by SMG1, readying $UPF1_{LL}$ to scaffold assembly of productive decay complexes (Kurosaki *et al*, 2014; Durand *et al*, 2016). In this scenario, mRNAs with a greater relative propensity to bind $UPF1_{LL}$ vs. $UPF1_{SL}$—those normally shielded by protective proteins—are thus poised to be decayed upon inhibition of translation. A second potential cause of transcript deprotection is that the location of the most frequently used stop codon changes, for example if termination at an unprotected stop codon at the end of an upstream ORF becomes more frequent than termination at a protected stop codon at the end of the main ORF.

This model is built on the fundamental concept that when translation is partially repressed, translation termination events still occur, but their relative frequencies across the transcriptome are expected to be altered. We show that diverse mechanisms of translation inhibition promote $UPF1_{LL}$ activity (Figs 5–7 and Fig EV4A–C), but our model predicts that the precise specificity of decay will be inhibitor-dependent. For example, the spectrum of termination events that occur upon inhibition of translation initiation is expected to be distinct from those that occur when elongation is blocked. Likewise, distinct cell types and growth conditions will have distinct translation termination landscapes, which will in turn lead to different collections of $UPF1_{LL}$ and $UPF1_{SL}$ targets. From a practical perspective, our data highlight the importance of careful control of cell growth conditions when studying $UPF1_{LL}$ and other aspects of NMD, as changes in translation due to differential nutrient availability, confluence, and other factors can negatively and positively affect decay in a substrate-specific manner.

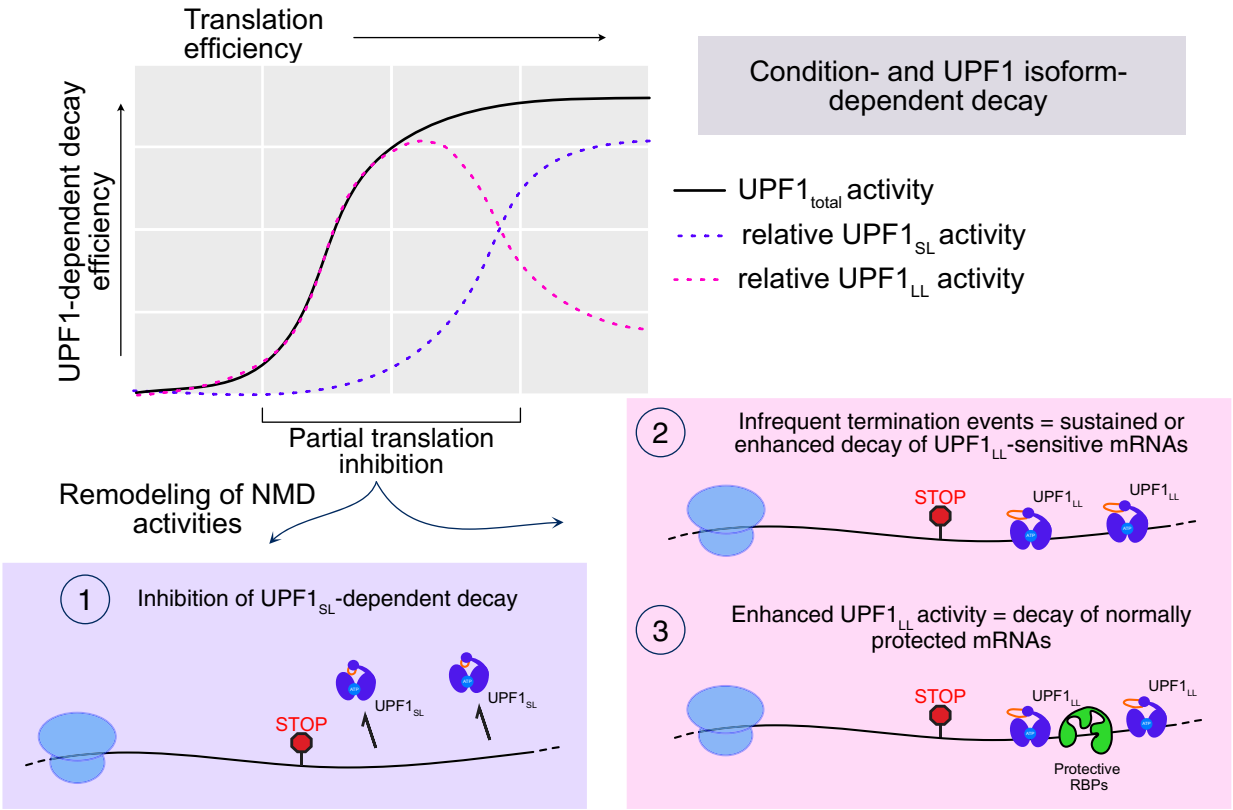

Figure 8. Translation efficiency and UPF1 isoform expression conditionally alter target susceptibility by the NMD pathway.
See Discussion for details.

The idea that the mammalian NMD pathway consists of multiple branches with distinct factor requirements and substrate specificities has been proposed by several groups, but the underlying mechanisms and regulatory roles of NMD branching are poorly understood (Gehring *et al*, 2005; Chan *et al*, 2007; Huang *et al*, 2011; Yi *et al*, 2021). Unraveling NMD pathway branches has been challenging, in part because most NMD proteins are essential for cell viability, precluding conclusive demonstrations that they are dispensable for decay of any given NMD target mRNA (Kishor *et al*, 2019a; Boehm *et al*, 2021; Yi *et al*, 2021). Our identification of differential activities of $UPF1_{SL}$ and $UPF1_{LL}$ is an unforeseen example of NMD pathway branching, which can be controlled at the cellular level by changes in the abundance of protective RBPs, translation, or UPF1 splicing. The differential regulation of $UPF1_{LL}$-dependent targets in $SMG7^{ko}$/$SMG6^{kd}$ and $SMG7^{ko}$/$SMG5^{kd}$ cells provides an initial indication that previously described NMD branches may be distinctly influenced by $UPF1_{LL}$ (Figs 1D and EV1E and F; (Boehm *et al*, 2021).

Because altered translation efficiency and induction of cellular stress pathways are pervasive in cancer, genetic disease, and infection, the expanded scope of $UPF1_{LL}$-dependent decay has far-reaching implications for the physiological roles of the mammalian NMD pathway in health and disease. In particular, the ability of $UPF1_{LL}$ to target specific mRNAs in response to translational repression positions NMD to function as a mechanism to reset the transcriptome upon cellular stress. The extent to which $UPF1_{LL}$ complements or collaborates with IRE1-mediated mRNA decay or the recently identified ER-associated NMD factor NBAS will require further study (Hollien & Weissman, 2006; Longman *et al*, 2020), but our data suggest that $UPF1_{LL}$ may help to relieve proteotoxic stress by reducing the abundance of transcripts encoding proteins with complex biosynthetic needs.

Even in the absence of stress, cells and tissues *in vivo* likely have lower basal rates of translation than those attained in exponentially growing transformed cell lines. Based on our findings, understanding how NMD shapes gene expression in diverse physiological contexts will require not just analysis of NMD targets characterized in transformed cells, but also transcripts that are conditionally targeted in response to changing translational states. Notably, we find that $UPF1_{LL}$ is able to conditionally regulate several proteins of central importance in cancer and other diseases, including fragile X mental retardation 1 (FMR1), the low-density lipoprotein receptor (LDLR), and oncogenes PTEN, EIF5A2, and ERBB2, among others (Goldstein & Brown, 2009; Song *et al*, 2012; Mathews & Hershey, 2015; Dockendorff & Labrador, 2019; Harbeck *et al*, 2019). Along with EIF5A2 and FMR1, several additional $UPF1_{LL}$ targets that undergo enhanced downregulation upon translational repression are themselves important regulators of translation and mRNA decay, including the signal recognition particle receptor SRPR, the major mRNA decapping enzyme DCP2, and the miRNA-processing endonuclease DICER1 (Akopian *et al*, 2013; Mugridge *et al*, 2018; Michlewski & Cáceres, 2019).

Materials and Methods

UPF1 isoform nomenclature

$UPF1_{SL}$ refers to the protein encoded by Ensembl transcript ID ENST00000262803.9 and $UPF1_{LL}$ by Ensembl transcript ID ENST00000599848.5. These isoforms are also referred to as UPF1 isoform 2 and UPF1 isoform 1, respectively (Nicholson *et al*, 2014; Gowravaram *et al*, 2018).

In vitro helicase assays

Unwinding assays were performed as previously described in detail (Fritz *et al*, 2020). Briefly, 75 nM of the pre-assembled RNA duplex substrate (described below) was combined with 1× unwinding reaction buffer (10 mM MES pH 6.0, 50 mM KOAc, 0.1 mM EDTA), 2 mM MgOAc, and 1-unit RNasin in a well of a half-area, black, flat-bottom 96-well plate (Corning 3993). PTBP1 (80 nM) was then added, the sample mixed, and incubated at room temperature for 10 min. Then, UPF1 (80 nM) was added, the sample mixed, and incubated at room temperature for 10 min. Finally, BHQ1 quencher (0.56 μM final; GTGTGCGTACAACTAGCT/3BHQ_1) and 2 mM ATP were added to initiate the unwinding reaction. An Infinite^{R} F200 Pro microplate reader and associated i-control^{TM} 1.9 software (Tecan) was used to monitor Alexa Fluor 488 fluorescence every 10 s for 20 min at 37°C. Measured fluorescence intensities were normalized to the zero timepoint for each condition to obtain relative fluorescence values. Four technical replicates for each condition were obtained at the same time. The decrease in fluorescence caused by UPF1 unwinding in the absence of PTBP1 at the end of each 20-min timecourse was used to calculate the time to 50% maximal unwinding and relative total unwinding for each condition. Because measurements were taken at 10-s intervals, the earliest time at which 50% maximal unwinding was observed is indicated on each graph.

To generate the RNA duplex, a DNA oligo template (5' TAATAC GACTCACTATAGGGACACAAAACAAAAGACAAAAAACACAAAACAA AAGACAAAAACACAAAACAAAAGACAAAAAGCCTCTCCTTCTCTC TGCTTCTCTCTCGCTGTGTGCGTACAACTAGCT 3') was PCR-amplified and then *in vitro* transcribed using the MEGAshortscript^{TM} T7 Transcription kit (Invitrogen). An 11:7 ratio of the helicase RNA substrate to 5' Alex Fluor 488 fluorescent oligo strand (Alexa Fluor 488/AGCTAGTTGTACGCACAC) was incubated with 2 mM MgOAC and 1× unwinding reaction buffer at 95°C for 3 min and 30 s and then slowly cooled to 30°C. All DNA oligos were obtained from Integrated DNA Technologies. The 5' fluorescent oligo probe and 3' BHQ1 quencher were acquired as RNase-free, HPLC-purified.

Cloning, expression, and purification of recombinant $UPF1_{LL}$ΔCH, $UPF1_{SL}$ΔCH, and PTBP1 were conducted as previously described (Gowravaram *et al*, 2018; Fritz *et al*, 2020). In this study, $UPF1_{LL}$ΔCH was purified in the same manner as $UPF1_{SL}$ΔCH (Fritz *et al*, 2020).

Mammalian cell lines and generation of CLIP-UPF1 expression lines

HEK-293 cells used in the endogenous $UPF1_{LL}$ knockdown and RNA-seq experiments were received from ATCC (CRL-3216) and maintained at 37°C and 5% CO_2 in DMEM with 10% FBS (Gibco) and 1% pen/strep. Stable integration of CLIP-$UPF1_{SL}$ into human Flp-In^{TM} T-Rex^{TM}-293 cells (Invitrogen) and subsequent maintenance of this stable line was previously described (Kishor *et al*, 2020). CLIP-$UPF1_{LL}$ expression lines were generated and maintained in an

identical manner. Total UPF1 and SMG6 depletion studies followed by RT–qPCR as well as the Roadblock-qPCR experiments were performed using HEK-293 cells maintained as described above. Total UPF1 depletion and RNA-seq was conducted using parental Flp-In™ T-Rex™-293 cells (Invitrogen) maintained according to manufacturer instructions. To express CLIP-UPF1 at levels ~0.7-fold that of the endogenous protein, the CMV promoter and 5' UTR hairpin from pcDNA HP40GFPTP (Hogg & Goff, 2010) were inserted in place of the tet-regulated pFRT/TO promoter in the CLIP-UPF1 expression plasmid (Kishor *et al*, 2020) via SpeI and HindIII sites. Stable cell lines Flp-In™ T-Rex™-293 in which the resulting UPF1 expression plasmids were integrated were prepared and maintained as above.

Endogenous UPF1, SMG6, or SRSF1 depletion by siRNA

The following siRNAs were used to deplete indicated UPF1 isoforms, SMG6, or SRSF1: total UPF1 (Forward sequence: 5' CUAC CAGUACCAGAACAUA 3'; Reverse sequence: 5' UAUGUUCUGGUA CUGGUAG 3'); $UPF1_{LL}$ (Forward sequence: 5' GGUAAUGAGGAUUU AGUCA 3'; Reverse sequence: 5' UGACUAAAUCCUCAUUACC 3'); SMG6 (Forward sequence: 5' GCUGCAGGUUACUUACAAG 3'; Reverse sequence: 5' CUUGUAAGUAACCUGCAGC 3'; Durand *et al*, 2016); SRSF1 (Forward sequence: 5' UGAAGCAGGUGAUGUAUGU 3'; Reverse sequence: 5' ACAUACAUCACCUGCUUCA 3'; (de Miguel *et al*, 2014)).

CLIP-UPF1 overexpression RIP-seq and RNA-seq

$CLIP\text{-}UPF1_{SL}$ overexpression RIP-seq and RNA-seq sample preparation were previously reported (Kishor *et al*, 2020); $CLIP\text{-}UPF1_{LL}$ datasets were generated in parallel. Briefly, CLIP-UPF1 stable cell lines or a GFP-expressing control line were seeded in 6 × 15 cm plates and then treated with 200 ng/ml doxycycline hyclate (Sigma) for 48 h to induce CLIP-UPF1 expression. Cells were harvested 48 h post-induction at 80–85% confluency and whole cell lysate generated by the freeze/thaw method as previously described (Hogg & Collins, 2007a, 2007b; Hogg & Goff, 2010; Fritz *et al*, 2018). Equilibrated cell extracts, reserving $1/10^{th}$ for downstream input analysis, were then combined with 10 μM CLIP-Biotin (New England Biolabs) and rotated (end-over-end) for 1 h at 4°C to allow CLIP-UPF1 to react with the CLIP-Biotin substrate and yield covalently biotinylated protein. Unbound CLIP-Biotin was subsequently removed by passing the samples through Zeba™ Spin Desalting Columns, 40K MWCO, 2 ml (Thermo Scientific) according to manufacturer instructions. Buffer exchange was performed with HLB-150 supplemented with 1 mM DTT and 0.1% NP-40. Pre-washed Dynabeads™ MyOne™ Streptavidin T1 (Invitrogen) were then added, and the samples rotated (end-over-end) for 1 h at 4°C to immobilize the biotin-bound CLIP-UPF1 complexes. The samples were then washed three times with 500 μL of HLB-150 supplemented with 1 mM DTT and 0.1% NP-40 and $1/100^{th}$ reserved for downstream Western blot analysis of CLIP-UPF1 pull-down efficiency. The remainder was combined with TRIzol™ (Invitrogen) and RNA was isolated according to manufacturer instructions. DNase treatment was subsequently performed using RQ1 RNase-Free DNase (Promega), and RNA was isolated by acid phenol chloroform extraction. This resulted in approximately 1 μg of total RNA that was then subjected to high-throughput sequencing. In parallel, the reserved input lysate (approximately 3 μg of total RNA) was also sent for high-throughput sequencing. A total of three biological replicates from each condition were processed. Sequencing libraries were prepared from input and bound RNA using the Illumina TruSeq Stranded Total RNA Human kit and sequenced on an Illumina HiSeq 3000 instrument.

To validate select transcripts by RT–qPCR, an equivalent volume of reserved RNA (3 μl) was used as a template for cDNA synthesis using the Maxima First Strand cDNA synthesis kit for RT–qPCR (Thermo Scientific) according to manufacturer instructions. The resulting cDNA was diluted with nuclease-free water and subsequently analyzed by qPCR using iTaq Universal SYBR Green Supermix (Bio-Rad) on a Roche LightCycler 96 instrument (Roche). Sequences for gene-specific primers used for amplification are listed in Appendix Table S2. For input samples, relative fold change was determined by calculating $2^{-\Delta\Delta CT}$ values using GAPDH for normalization. For pull-down samples, relative fold enrichment was determined by dividing the C_q value of the pull-down by its corresponding input, multiplying by 100 and then normalizing to the relative recovery of the SMG1 transcript.

For assessment of CLIP-UPF1 expression and pull-down efficiency by Western blot, reserved input and IP samples were run on a NuPage™ 4–12% Bis-Tris Protein Gel (Invitrogen) using MOPS buffer according to manufacturer instructions and subsequently transferred to a nitrocellulose membrane according to the NuPage™ manufacturer's protocol (Invitrogen). Membranes were incubated with a blocking buffer for fluorescent Western blotting (Rockland) for 1 h at room temperature and then incubated overnight at 4°C with the indicated primary antibody. Primary antibodies used: anti-RENT1 (goat polyclonal, Bethyl, A300-038A, 1:1,000) and anti-β-actin (mouse monoclonal, Cell Signaling, #3700, 1:1,000). Membranes were subsequently washed three times with 1 × TBS supplemented with 0.1% Tween-20 and then incubated with the appropriate secondary antibody for 1 h at room temperature. Secondary antibodies used: anti-goat IgG (H&L) Antibody DyLight™ 680 Conjugated (Rockland, 605-744-002, 1:10,000) and anti-mouse IgG (H&L) Antibody DyLight™ 680 Conjugated (Rockland, 610-744-124, 1:10,000). Membranes were washed three times with 1 × TBS supplemented with 0.1% Tween-20 and then two times with 1 × TBS. Western blot images were obtained on an Amersham Typhoon imaging system (GE Healthcare Life Sciences) and quantified using ImageStudio software (LI-COR Biosciences).

For total UPF1 or SRSF1 depletion and rescue with CLIP-UPF1, 3×10^5 cells from the CLIP-UPF1 stable cell lines, which were engineered as resistant to the described total UPF1 siRNA, or the GFP-expressing control line were reverse transfected with 40 nM of a NT, pan-UPF1, or SRSF1-specific siRNA (described above) using Lipofectamine RNAiMAX according to manufacturer instructions. The next day, cells were treated with 200 ng/ml doxycycline hyclate (Sigma) for 48 h to induce expression of CLIP-UPF1. Cells were harvested 48 h post-induction, and total RNA was isolated using TRIzol™ (Invitrogen) according to manufacturer instructions. DNase treatment was subsequently performed using RQ1 RNase-Free DNase (Promega), and RNA was isolated by acid phenol chloroform extraction according to standard protocol. RT–qPCR was performed as described above.

Total UPF1 depletion and RNA-seq

3×10^5 HEK-293 cells (Invitrogen) were reverse transfected with 40 nM of a NT or UPF1-specific siRNA that targets both UPF1 isoforms (described above) using Lipofectamine RNAiMAX according to manufacturer instructions. Seventy-two hours post-siRNA transfection, total RNA was isolated using TRIzol™ (Invitrogen) according to manufacturer instructions. DNase-treatment was subsequently performed using RQ1 RNase-Free DNase (Promega), and RNA was isolated by acid phenol chloroform extraction according to standard protocol. A total of 2 μg RNA was then subjected to high-throughput sequencing. Three replicates were processed for each condition. Sequencing libraries were prepared using the Illumina TruSeq Stranded Total RNA Human kit and sequenced on an Illumina NovaSeq 6000 instrument.

Total UPF1 and SMG6 depletion with RT–qPCR

3×10^5 HEK-293 cells were reverse transfected with 40 nM of a NT, total UPF1, or SMG6-specific siRNA (described above) using Lipofectamine RNAiMAX according to manufacturer instructions. Forty-eight hours post-siRNA transfection, cells were replated at a density of 5×10^5 cells per well of a 6-well plate. This step was critical to achieve 70–75% confluency on the day of drug treatment (if applicable) and cell harvest. The next day, cells were directly harvested or treated with 50 μg/ml puromycin (Sigma) for 4 h. A total of three replicates were generated for each condition. Total RNA was then isolated using TRIzol™ (Invitrogen) according to manufacturer instructions. DNase treatment was subsequently performed using RQ1 RNase-Free DNase (Promega), and RNA was isolated by acid phenol chloroform extraction according to standard protocol. For RT–qPCR, 500 ng of total RNA was used as input for cDNA synthesis using the Maxima First Strand cDNA synthesis kit for RT–qPCR (Thermo Scientific) according to manufacturer instructions. The resulting cDNA was diluted with nuclease-free water and subsequently analyzed by qPCR using iTaq Universal SYBR Green Supermix (Bio-Rad) on a Roche LightCycler 96 instrument (Roche). Sequences for gene-specific primers used for amplification are listed in Appendix Table S2. Relative fold changes were determined by calculating $2^{-\Delta\Delta CT}$ values using GAPDH for normalization.

Endogenous $UPF1_{LL}$ knockdown with puromycin or thapsigargin treatment and RNA-seq

3×10^5 HEK-293 cells were reverse transfected with 40 nM of a NT or $UPF1_{LL}$-specific siRNA (described above) using Lipofectamine RNAiMAX according to manufacturer instructions. Forty-eight hours post-siRNA transfection, cells were replated at a density of 5×10^5 cells per well of a 6-well plate. The next day, cells were treated with vehicle control, 25, 50, or 100 μg/ml puromycin (Sigma) for 4 h, or 1 μM thapsigargin for 6 or 9 h. A total of three replicates were generated for each condition. Total RNA was then isolated using the RNeasy Plus Mini Kit (QIAGEN). Sequencing libraries were prepared from 2 μg total RNA using the Illumina TruSeq Stranded Total RNA Human kit and sequenced on an NovaSeq 6000 instrument. For RT–qPCR validation of changes in target gene expression, 500 ng of total RNA was used as input for cDNA synthesis using the Maxima First Strand cDNA synthesis kit for RT–qPCR (Thermo Scientific) according to manufacturer instructions. The resulting cDNA was diluted with nuclease-free water and subsequently analyzed by qPCR using iTaq Universal SYBR Green Supermix (Bio-Rad) on a Roche LightCycler 96 instrument (Roche). Sequences for gene-specific primers used for amplification are listed in Appendix Table S2. Relative fold changes were determined by calculating $2^{-\Delta\Delta CT}$ values using GAPDH for normalization.

Roadblock-qPCR to measure endogenous mRNA stability

mRNA decay measurements were determined using Roadblock-qPCR as previously described (Watson *et al*, 2021) but with the following adaptations. 3×10^5 HEK-293 cells were reverse transfected with 40 nM of a NT or $UPF1_{LL}$-specific siRNA (described above) using Lipofectamine RNAiMAX according to manufacturer instructions. Forty-eight hours post-siRNA transfection, cells were replated at a density of 5×10^5 cells per well of a 6-well plate. The next day, cells were treated with 400 μM 4-thiouridine (4sU; Cayman Chemical) and vehicle control or 50 μg/ml puromycin (Sigma) for a total of 4 h. Cells were harvested at indicated timepoints and total RNA was isolated using TRIzol™ (Invitrogen) according to manufacturer instructions, but with the addition of 1 mM (final) DTT to the isopropanol precipitation in order to maintain 4sU in a reduced state (Schofield *et al*, 2018). Isolated RNA from 4sU-exposed cells was treated with 48 mM N-ethylmaleimide (NEM; Sigma) as described by Watson *et al* and then purified using RNAClean XP beads (Beckman Coulter) according to manufacturer instructions. A total of 1 μg RNA was used as input for cDNA synthesis with oligo dT_{18} primers and Protoscript II reverse transcriptase (New England BioLabs) according to manufacturer instructions. The resulting cDNA was diluted with nuclease-free water and subsequently analyzed by qPCR using iTaq Universal SYBR Green Supermix (Bio-Rad) on a Roche LightCycler 96 instrument (Roche). Sequences for gene-specific primers used for amplification are listed in Appendix Table S2. Relative fold changes were determined by calculating $2^{-\Delta\Delta CT}$ values using time 0 as the reference and GAPDH for normalization. mRNA half-lives were estimated by fitting the data to a single-phase exponential decay model using GraphPad Prism 9.1.0.

Western for phospho-eIF2α

HEK-293 cells treated with 1 μM thapsigargin were lysed in 1X Passive Lysis Buffer (Promega) supplemented with Halt™ Protease and Phosphatase Inhibitor Cocktail (Thermo Scientific) according to manufacturer instructions. A total of 5 μg protein was run on a NuPage™ 4–12% Bis-Tris Protein Gel (Invitrogen) using MOPS buffer according to manufacturer instructions and subsequently transferred to a nitrocellulose membrane according to the NuPage™ manufacturer's protocol (Invitrogen). Detection of phospho and total eIF2α was performed as previously described (Young-Baird *et al*, 2020).

Semiquantitative PCR to detect UPF1 isoform ratios

Generated cDNA ($1/40^{th}$) from RNA-seq samples was used as input for PCR amplification with Phusion High-Fidelity DNA polymerase (New England Biolabs) and UPF1-specific primers that flank the regulatory loop sequence (Forward: 5' AACAAGCTGGAGGAGCT

GTGGA 3'; Reverse: 5' ACTTCCACACAAAATCCACCTGGAAGTT 3'). The PCR cycling conditions used were an initial denaturation at 98°C for 30 s and then 22 cycles of 98°C for 10 s, 63°C for 30 s, and 72°C for 15 s. PCR products were then run on a 8% Novex™ TBE gel (Invitrogen) according to manufacturer instructions and subsequently stained with SYBR® Gold Nucleic Acid Stain (Invitrogen). Images were obtained on an Amersham Typhoon imaging system (GE Healthcare Life Sciences) and quantified using ImageStudio software (LI-COR Biosciences).

Gene-level differential expression analysis

For analysis of RNA-seq data from HEK-293 cells treated with NT, anti-$UPF1_{total}$, or anti-$UPF1_{LL}$ siRNAs, raw fastq reads from the NovaSeq 6000 platform were trimmed with fastp (Chen *et al*, 2018), with the parameters --detect_adapter_for_pe and --trim_poly_g. Trimmed reads were aligned with HISAT2 to the hg19/GRCh37 genome and transcriptome index provided by the authors (Kim *et al*, 2019). For gene-level differential expression analysis of in-house and published datasets, reads mapping to Ensembl GRCh37 release 75 gene annotations were quantified with featureCounts (Liao *et al*, 2014), and differential gene expression was analyzed using limma/voom, as implemented by the Degust server (Powell, 2015; Ritchie *et al*, 2015). GO analysis was performed with DAVID Bioinformatics Resources, using UniProt keyword classifiers and genes that were represented by > 0.5 transcripts per million (TPM) in the RNA-seq datasets as a background set (Huang *et al*, 2009a, 2009b; UniProt Consortium, 2021). All comparisons among datasets were performed using genes with average TPM > 0.5 in all datasets. Analysis of data from (Boehm *et al*, 2021) was performed using the authors' analysis of RNA-seq of $SMG7^{ko}$ line 34; similar results were observed with $SMG7^{ko}$ line 2.

Isoform-level differential expression analysis

For isoform-level differential expression analysis, trimmed reads were quantified against a custom HEK-293 transcriptome index, prepared with Stringtie and TACO as described (Pertea *et al*, 2015; Niknafs *et al*, 2017; Kishor *et al*, 2019b), using kallisto software with parameters --bias -b 1000 -t 16 --single --rf-stranded -l 200 -s 20 (Bray *et al*, 2016). Differential transcript expression analysis was performed using RUVSeq and edgeR (Robinson *et al*, 2009; Risso *et al*, 2014). Normalization and batch correction were performed with the RUVg function, based on transcripts with invariant expression among all samples. The edgeR TMM method was used to obtain normalized differential expression values and to calculate FDRs. Differential isoform usage was calculated for the most abundant PTC and non-PTC isoforms of each gene using IsoformSwitchAnalyzer and the DEXSeq package (Anders *et al*, 2012; Vitting-Seerup & Sandelin, 2019). Alternative splicing was analyzed using rMATS 4.0.1 (Shen *et al*, 2014), and Sashimi plots were generated using Integrative Genomics Viewer 2.8.2 (Thorvaldsdóttir *et al*, 2013). ENCODE rMATS data were downloaded from: https://github.com/YeoLab/rbp-maps (Yee *et al*, 2019).

Analysis of mRNA features

IsoformSwitchAnalyzeR was used to annotate PTCs in the custom HEK-293 transcriptome, as described (Kishor *et al*, 2019b; Vitting-Seerup & Sandelin, 2019). For PTC analysis, IsoformSwitchAnalyzeR orfMethod "longest" setting was used to predict the longest ORF (min. 100 nt) in each annotated transcript, and TCs located > 50 nt upstream of the final exon junction were designated potential PTCs. Genes represented by at least one transcript predicted to contain a TC within 50 nt of the final exon junction or in the last exon and at least one transcript predicted to contain a PTC, defined as a TC more than 50 nt upstream of the final exon junction, were selected for analysis of differential isoform usage upon total UPF1 and $UPF1_{LL}$-specific knockdown in Appendix Fig S1C. Putative uORFs were identified using the IsoformSwitchAnalyzeR orfMethod "mostUpstream" setting (min. length 60 nt). ORFs predicted by this method that were upstream of the longest predicted ORF were designated potential uORFs. For Appendix Table S1, genes were assigned as PTC- or uORF-containing if at least one transcript with > 0.5 TPM in all $siUPF1_{total}$, $siUPF1_{LL}$, and siNT samples was found to have a putative PTC or uORF.

The most abundant transcript isoform from each gene, as determined by quantification with kallisto as above, was used for analysis of 3'UTR length and PTBP1 and hnRNP L binding motif positions and frequencies. PTBP1 and hnRNP L binding motif position-specific scoring matrices were downloaded from the RBPmap database and used for motif finding in 3'UTRs derived from the custom HEK-293 transcriptome with HOMER, as described (Heinz *et al*, 2010; Paz *et al*, 2014; Kishor *et al*, 2019b).

RIP-seq analysis

Raw fastq reads from CLIP-UPF1 overexpression RNA-seq and RIP-seq data were trimmed with Cutadapt using the following parameters: --times 2 -e 0 -O 5 --quality-cutoff 6 -m 18 -a AGATCGGAAGAGCACACGTCTGAACTCCAGTCAC -A AGATCGGAAGAGCGTCGTGTAGGGAAAGAGTGTAGATCTCGGTGGTCGCCGTATCATT -b AAAAAAAAAAAAAAAAAAAAAAAAAAAAAAAAAAAAAAAAAAAA -b TTTTTTTTTTTTTTTTTTTTTTTTTTTTTTTTTTTTTTTTTTTT (Martin, 2011). Trimmed reads were quantified using kallisto software with parameters --bias -b 1000 -t 16 -single --rf-stranded -l 200 -s 20 (Bray *et al*, 2016). RIP-seq enrichment values were obtained by dividing TPM values from IP samples by TPM values from input samples.

GTEx data analysis

GTEx data were downloaded from the GTEx Portal on 11/11/2020. To determine the relative representation of $UPF1_{LL}$ and $UPF1_{SL}$ mRNA isoforms, transcript TPM values for transcript ENST00000599848.5 ($UPF1_{LL}$) were divided by the total TPM values derived from transcripts ENST00000599848.5 ($UPF1_{LL}$) and ENST00000262803.9 ($UPF1_{SL}$). GTEx samples were assigned to the indicated tissue types using the sample attributes provided in GTEx Analysis v8.

Statistical analysis

Statistics and exponential decay fits were calculated using GraphPad Prism 9. Density plots were generated using the JMP 14 (SAS Institute) One-way Platform, with default values. All statistical tests were two-sided, and all replicates shown from cell-based experiments are biological replicates, defined as experiments performed

with independently manipulated cell populations. For helicase assays, biological replicates are defined as biochemical assays performed with independent reaction mixtures at different times and technical replicates are defined as reactions performed at the same time. Where indicated in the figure legends, *P*-values are reported in Dataset EV3.

Data availability

- RNA-Seq data: Gene Expression Omnibus GSE134059 (https://www.ncbi.nlm.nih.gov/geo/query/acc.cgi?acc=GSE134059).
- RNA-Seq data: Gene Expression Omnibus GSE162699 (https://www.ncbi.nlm.nih.gov/geo/query/acc.cgi?acc=GSE162699).
- RNA-Seq data: Gene Expression Omnibus GSE176197 (https://www.ncbi.nlm.nih.gov/geo/query/acc.cgi?acc=GSE176197).

Expanded View for this article is available online.

Acknowledgements
We thank Sutapa Chakrabarti for the UPF1$_{LL}$ΔCH recombinant expression plasmid and members of the Hogg laboratory and Nicholas R. Guydosh for critical reading of the manuscript. We are grateful to Sandy Mattijssen and Richard J. Maraia for helpful discussion and to Sara K. Young-Baird for thapsigargin reagents, helpful discussion, and assistance with phospho-eIF2α immunoblotting. High-throughput sequencing was conducted by Yan Luo and Poching Liu in the NHLBI DNA Sequencing and Genomics Core. The Genotype-Tissue Expression (GTEx) Project was supported by the Common Fund of the Office of the Director of the National Institutes of Health, and by NCI, NHGRI, NHLBI, NIDA, NIMH, and NINDS. This work was supported by the Intramural Research Program, National Institutes of Health, National Heart, Lung, and Blood Institute and utilized the computational resources of the NIH HPC Biowulf cluster (http://hpc.nih.gov).

Author contributions
Sarah E Fritz: Conceptualization; Data curation; Formal analysis; Investigation; Visualization; Writing—original draft; Writing—review and editing. **Soumya Ranganathan:** Investigation; Methodology; Writing—review and editing. **Clara D Wang:** Investigation; Writing—review and editing. **J Robert Hogg:** Conceptualization; Data curation; Formal analysis; Supervision; Funding acquisition; Investigation; Writing—original draft; Project administration; Writing—review and editing.

In addition to the CRediT author contributions listed above, the contributions in detail are:

SEF and JRH conceived and designed the study, analyzed and interpreted the data, and wrote the manuscript. SEF acquired the UPF1 RIP-seq and RNA-seq data and performed associated cellular studies. SR acquired the unwinding data. CDW performed the total UPF1 knockdown for RNA-seq. All authors read and approved the manuscript.

Disclosure and competing interests statement
The authors declare that they have no conflict of interest.

References

Akopian D, Shen K, Zhang X, Shan S-O (2013) Signal recognition particle: an essential protein-targeting machine. *Annu Rev Biochem* 82: 693 – 721

Alkallas R, Fish L, Goodarzi H, Najafabadi HS (2017) Inference of RNA decay rate from transcriptional profiling highlights the regulatory programs of Alzheimer's disease. *Nat Commun* 8: 1 – 11

Anders S, Reyes A, Huber W (2012) Detecting differential usage of exons from RNA-seq data. *Genome Res* 22: 2008 – 2017

Ashburner M, Ball CA, Blake JA, Botstein D, Butler H, Cherry JM, Davis AP, Dolinski K, Dwight SS, Eppig JT *et al* (2000) Gene ontology: tool for the unification of biology. The Gene Ontology Consortium. *Nat Genet* 25: 25 – 29

Baird TD, Wek RC (2012) Eukaryotic initiation factor 2 phosphorylation and translational control in metabolism. *Adv Nutr* 3: 307 – 321

Baker SL, Hogg JR (2017) A system for coordinated analysis of translational readthrough and nonsense-mediated mRNA decay. *PLoS One* 12: e0173980

Boehm V, Kueckelmann S, Gerbracht JV, Kallabis S, Britto-Borges T, Altmüller J, Krüger M, Dieterich C, Gehring NH (2021) SMG5-SMG7 authorize nonsense-mediated mRNA decay by enabling SMG6 endonucleolytic activity. *Nat Commun* 12: 1 – 19

Bray NL, Pimentel H, Melsted P, Pachter L (2016) Near-optimal probabilistic RNA-seq quantification. *Nat Biotechnol* 34: 525 – 527

Caputi M, Clark E, Paz S (2019) Gene Expression Omnibus GSE124397 (https://www.ncbi.nlm.nih.gov/geo/query/acc.cgi?acc=GSE124397). [DATASET]

Carter MS, Doskow J, Morris P, Li S, Nhim RP, Sandstedt S, Wilkinson MF (1995) A regulatory mechanism that detects premature nonsense codons in T-cell receptor transcripts *in vivo* is reversed by protein synthesis inhibitors *in vitro*. *J Biol Chem* 270: 28995 – 29003

Causier B, Li Z, De Smet R, Lloyd JPB, Van de Peer Y, Davies B (2017) Conservation of nonsense-mediated mRNA decay complex components throughout eukaryotic evolution. *Sci Rep* 7: 1 – 12

Chakrabarti S, Jayachandran U, Bonneau F, Fiorini F, Basquin C, Domcke S, Le Hir H, Conti E (2011) Molecular mechanisms for the RNA-dependent ATPase activity of Upf1 and its regulation by Upf2. *Mol Cell* 41: 693 – 703

Chamieh H, Ballut L, Bonneau F, Le Hir H (2008) NMD factors UPF2 and UPF3 bridge UPF1 to the exon junction complex and stimulate its RNA helicase activity. *Nat Struct Mol Biol* 15: 85 – 93

Chan W-K, Huang L, Gudikote JP, Chang Y-F, Imam JS, MacLean II JA, Wilkinson MF (2007) An alternative branch of the nonsense-mediated decay pathway. *EMBO J* 26: 1820 – 1830

Chen S, Zhou Y, Chen Y, Gu J (2018) fastp: an ultra-fast all-in-one FASTQ preprocessor. *Bioinformatics* 34: i884 – i890

Cheng Z, Muhlrad D, Lim MK, Parker R, Song H (2007) Structural and functional insights into the human Upf1 helicase core. *EMBO J* 26: 253 – 264

Colombo M, Karousis ED, Bourquin J, Bruggmann R, Mühlemann O (2017) Transcriptome-wide identification of NMD-targeted human mRNAs reveals extensive redundancy between SMG6- and SMG7-mediated degradation pathways. *RNA* 23: 189 – 201

Costa-Mattioli M, Walter P (2020) The integrated stress response: From mechanism to disease. *Science* 368: eaat5314

Czaplinski K, Weng Y, Hagan KW, Peltz SW (1995) Purification and characterization of the Upf1 protein: a factor involved in translation and mRNA degradation. *RNA* 1: 610 – 623

Dockendorff TC, Labrador M (2019) The fragile X protein and genome function. *Mol Neurobiol* 56: 711 – 721

Durand S, Franks TM, Lykke-Andersen J (2016) Hyperphosphorylation amplifies UPF1 activity to resolve stalls in nonsense-mediated mRNA decay. *Nat Commun* 7: 1 – 12

Eberle AB, Lykke-Andersen S, Mühlemann O, Jensen TH (2009) SMG6 promotes endonucleolytic cleavage of nonsense mRNA in human cells. *Nat Struct Mol Biol* 16: 49 – 55

Eden E, Navon R, Steinfeld I, Lipson D, Yakhini Z (2009) GOrilla: a tool for discovery and visualization of enriched GO terms in ranked gene lists. *BMC Bioinformatics* 10: 1 – 7

Fiorini F, Bonneau F, Le Hir H (2012) Biochemical characterization of the RNA helicase UPF1 involved in nonsense-mediated mRNA decay. *Methods Enzymol* 511: 255 – 274

Fiorini F, Boudvillain M, Le Hir H (2013) Tight intramolecular regulation of the human Upf1 helicase by its N- and C-terminal domains. *Nucleic Acids Res* 41: 2404 – 2415

Franks TM, Singh G, Lykke-Andersen J (2010) Upf1 ATPase-dependent mRNP disassembly is required for completion of nonsense- mediated mRNA decay. *Cell* 143: 938 – 950

Fritz SE, Haque N, Hogg JR (2018) Highly efficient *in vitro* translation of authentic affinity-purified messenger ribonucleoprotein complexes. *RNA* 24: 982 – 989

Fritz SE, Ranganathan S, Wang CD, Hogg JR (2020) The RNA-binding protein PTBP1 promotes ATPase-dependent dissociation of the RNA helicase UPF1 to protect transcripts from nonsense-mediated mRNA decay. *J Biol Chem* 295: 11613 – 11625

Gautier A, Juillerat A, Heinis C, Corrêa Jr IR, Kindermann M, Beaufils F, Johnsson K (2008) An engineered protein tag for multiprotein labeling in living cells. *Chem Biol* 15: 128 – 136

Ge Z, Quek BL, Beemon KL, Hogg JR (2016) Polypyrimidine tract binding protein 1 protects mRNAs from recognition by the nonsense-mediated mRNA decay pathway. *eLife* 5: e11155

Ge Z, Quek BL, Beemon KL, Hogg JR (2016) Gene Expression Omnibus GSE59884 (https://www.ncbi.nlm.nih.gov/geo/query/acc.cgi?acc=GSE59884). [DATASET]

Gehring NH, Kunz JB, Neu-Yilik G, Breit S, Viegas MH, Hentze MW, Kulozik AE (2005) Exon-junction complex components specify distinct routes of nonsense-mediated mRNA decay with differential cofactor requirements. *Mol Cell* 20: 65 – 75

Goetz AE, Wilkinson M (2017) Stress and the nonsense-mediated RNA decay pathway. *Cell Mol Life Sci* 74: 3509 – 3531

Goldstein JL, Brown MS (2009) The LDL receptor. *Arterioscler Thromb Vasc Biol* 29: 431 – 438

Gowravaram M, Bonneau F, Kanaan J, Maciej VD, Fiorini F, Raj S, Croquette V, Le Hir H, Chakrabarti S (2018) A conserved structural element in the RNA helicase UPF1 regulates its catalytic activity in an isoform-specific manner. *Nucleic Acids Res* 46: 2648 – 2659

Harbeck N, Penault-Llorca F, Cortes J, Gnant M, Houssami N, Poortmans P, Ruddy K, Tsang J, Cardoso F (2019) Breast cancer. *Nat Rev Dis Primers* 5: 66

Heinz S, Benner C, Spann N, Bertolino E, Lin YC, Laslo P, Cheng JX, Murre C, Singh H, Glass CK (2010) Simple combinations of lineage-determining transcription factors prime cis-regulatory elements required for macrophage and B cell identities. *Mol Cell* 38: 576 – 589

Hodgkin J, Papp A, Pulak R, Ambros V, Anderson P (1989) A new kind of informational suppression in the nematode *Caenorhabditis elegans*. *Genetics* 123: 301 – 313

Hogg JR, Collins K (2007a) RNA-based affinity purification reveals 7SK RNPs with distinct composition and regulation. *RNA* 13: 868 – 880

Hogg JR, Collins K (2007b) Human Y5 RNA specializes a Ro ribonucleoprotein for 5S ribosomal RNA quality control. *Genes Dev* 21: 3067 – 3072

Hogg JR, Goff SP (2010) Upf1 senses 3′ UTR length to potentiate mRNA decay. *Cell* 143: 379 – 389

Hollien J, Weissman JS (2006) Decay of endoplasmic reticulum-localized mRNAs during the unfolded protein response. *Science* 313: 104 – 107

Huang DW, Sherman BT, Lempicki RA (2009a) Systematic and integrative analysis of large gene lists using DAVID bioinformatics resources. *Nat Protoc* 4: 44 – 57

Huang DW, Sherman BT, Lempicki RA (2009b) Bioinformatics enrichment tools: paths toward the comprehensive functional analysis of large gene lists. *Nucleic Acids Res* 37: 1 – 13

Huang L, Lou C-H, Chan W, Shum EY, Shao A, Stone E, Karam R, Song H-W, Wilkinson MF (2011) RNA homeostasis governed by cell type-specific and branched feedback loops acting on NMD. *Mol Cell* 43: 950 – 961

Huntzinger E, Kashima I, Fauser M, Saulière J, Izaurralde E (2008) SMG6 is the catalytic endonuclease that cleaves mRNAs containing nonsense codons in metazoan. *RNA* 14: 2609 – 2617

Hurt JA, Robertson AD, Burge CB (2013) Global analyses of UPF1 binding and function reveal expanded scope of nonsense-mediated mRNA decay. *Genome Res* 23: 1636 – 1650

Jan CH, Williams CC, Weissman JS (2014) Principles of ER cotranslational translocation revealed by proximity-specific ribosome profiling. *Science* 346: 1257521

Karousis ED, Mühlemann O (2019) Nonsense-mediated mRNA decay begins where translation ends. *Cold Spring Harb Perspect Biol* 11: a032862

Kashima I, Yamashita A, Izumi N, Kataoka N, Morishita R, Hoshino S, Ohno M, Dreyfuss G, Ohno S (2006) Binding of a novel SMG-1-Upf1-eRF1-eRF3 complex (SURF) to the exon junction complex triggers Upf1 phosphorylation and nonsense-mediated mRNA decay. *Genes Dev* 20: 355 – 367

Kearse MG, Goldman DH, Choi J, Nwaezeapu C, Liang D, Green KM, Goldstrohm AC, Todd PK, Green R, Wilusz JE (2019) Ribosome queuing enables non-AUG translation to be resistant to multiple protein synthesis inhibitors. *Genes Dev* 33: 871 – 885

Kearse M, Goldman D, Choi J, Nwaezeapu C, Liang D, Green K, Goldstrohm A, Todd P, Green R, Wilusz J (2019) Gene Expression Omnibus GSE125086 (https://www.ncbi.nlm.nih.gov/geo/query/acc.cgi?acc=GSE125086). [DATASET]

Keene JD (2007) RNA regulons: coordination of post-transcriptional events. *Nat Rev Genet* 8: 533 – 543

Kim D, Paggi JM, Park C, Bennett C, Salzberg SL (2019) Graph-based genome alignment and genotyping with HISAT2 and HISAT-genotype. *Nat Biotechnol* 37: 907 – 915

Kim YK, Maquat LE (2019) UPFront and center in RNA decay: UPF1 in nonsense-mediated mRNA decay and beyond. *RNA* 25: 407 – 422

Kishor A, Fritz SE, Hogg JR (2019a) Nonsense-mediated mRNA decay: the challenge of telling right from wrong in a complex transcriptome. *Wiley Interdiscip Rev RNA* 10: e1548

Kishor A, Fritz SE, Haque N, Ge Z, Tunc I, Yang W, Zhu J, Hogg JR (2020) Activation and inhibition of nonsense-mediated mRNA decay control the abundance of alternative polyadenylation products. *Nucleic Acids Res* 48: 7468 – 7482

Kishor A, Ge Z, Hogg JR (2019b) hnRNP L-dependent protection of normal mRNAs from NMD subverts quality control in B cell lymphoma. *EMBO J* 38: e99128

Kurosaki T, Li W, Hoque M, Popp MW-L, Ermolenko DN, Tian B, Maquat LE (2014) A post-translational regulatory switch on UPF1 controls targeted mRNA degradation. *Genes Dev* 28: 1900 – 1916

Lareau LF, Inada M, Green RE, Wengrod JC, Brenner SE (2007) Unproductive splicing of SR genes associated with highly conserved and ultraconserved DNA elements. *Nature* 446: 926 – 929

Lavysh D, Neu-Yilik G (2020) UPF1-Mediated RNA decay-danse macabre in a cloud. *Biomolecules* 10: 999

Le Hir H, Izaurralde E, Maquat LE, Moore MJ (2000a) The spliceosome deposits multiple proteins 20–24 nucleotides upstream of mRNA exon-exon junctions. *EMBO J* 19: 6860 – 6869

Le Hir H, Moore MJ, Maquat LE (2000b) Pre-mRNA splicing alters mRNP composition: evidence for stable association of proteins at exon-exon junctions. *Genes Dev* 14: 1098 – 1108

Lee SR, Pratt GA, Martinez FJ, Yeo GW, Lykke-Andersen J (2015) Target discrimination in nonsense-mediated mRNA decay requires Upf1 ATPase activity. *Mol Cell* 59: 413 – 425

Li Z, Vuong JK, Zhang M, Stork C, Zheng S (2017) Inhibition of nonsense-mediated RNA decay by ER stress. *RNA* 23: 378 – 394

Liao Y, Smyth GK, Shi W (2014) featureCounts: an efficient general purpose program for assigning sequence reads to genomic features. *Bioinformatics* 30: 923 – 930

Linares AJ, Lin C-H, Damianov A, Adams KL, Novitch BG, Black DL (2015) The splicing regulator PTBP1 controls the activity of the transcription factor Pbx1 during neuronal differentiation. *eLife* 4: e09268

Linares AJ, Lin CH, Damianov A, Adams KL, Novitch BG, Black D (2015) Gene Expression Omnibus GSE71179 (https://www.ncbi.nlm.nih.gov/geo/query/acc.cgi?acc=GSE71179). [DATASET]

Loh B, Jonas S, Izaurralde E (2013) The SMG5-SMG7 heterodimer directly recruits the CCR4-NOT deadenylase complex to mRNAs containing nonsense codons via interaction with POP2. *Genes Dev* 27: 2125 – 2138

Longman D, Jackson-Jones KA, Maslon MM, Murphy LC, Young RS, Stoddart JJ, Hug N, Taylor MS, Papadopoulos DK, Cáceres JF (2020) Identification of a localized nonsense-mediated decay pathway at the endoplasmic reticulum. *Genes Dev* 34: 1075 – 1088

Martin M (2011) Cutadapt removes adapter sequences from high-throughput sequencing reads. *EMBnet.journal* 17: 10 – 12

Martinez-Nunez RT, Sanford JR (2016) Gene Expression Omnibus GSE89774 (https://www.ncbi.nlm.nih.gov/geo/query/acc.cgi?acc=GSE89774). [DATASET]

Martinez-Nunez RT, Wallace A, Coyne D, Jansson L, Rush M, Ennajdaoui H, Katzman S, Bailey J, Deinhardt K, Sanchez-Elsner T *et al* (2017) Modulation of nonsense mediated decay by rapamycin. *Nucleic Acids Res* 45: 3448 – 3459

Mathews MB, Hershey JWB (2015) The translation factor eIF5A and human cancer. *Biochim Biophys Acta* 1849: 836 – 844

Michlewski G, Cáceres JF (2019) Post-transcriptional control of miRNA biogenesis. *RNA* 25: 1 – 16

de Miguel FJ, Sharma RD, Pajares MJ, Montuenga LM, Rubio A, Pio R (2014) Identification of alternative splicing events regulated by the oncogenic factor SRSF1 in lung cancer. *Cancer Res* 74: 1105 – 1115

Mugridge JS, Coller J, Gross JD (2018) Structural and molecular mechanisms for the control of eukaryotic 5'-3' mRNA decay. *Nat Struct Mol Biol* 25: 1077 – 1085

Nathans D (1964) Puromycin inhibition of protein synthesis: incorporation of puromycin into peptide chains. *Proc Natl Acad Sci USA* 51: 585 – 592

Ni JZ, Grate L, Donohue JP, Preston C, Nobida N, O'Brien G, Shiue L, Clark TA, Blume JE, Ares Jr M (2007) Ultraconserved elements are associated with homeostatic control of splicing regulators by alternative splicing and nonsense-mediated decay. *Genes Dev* 21: 708 – 718

Nicholson P, Josi C, Kurosawa H, Yamashita A, Mühlemann O (2014) A novel phosphorylation-independent interaction between SMG6 and UPF1 is essential for human NMD. *Nucleic Acids Res* 42: 9217 – 9235

Nickless A, Jackson E, Marasa J, Nugent P, Mercer RW, Piwnica-Worms D, You Z (2014) Intracellular calcium regulates nonsense-mediated mRNA decay. *Nat Med* 20: 961 – 966

Niknafs YS, Pandian B, Iyer HK, Chinnaiyan AM, Iyer MK (2017) TACO produces robust multisample transcriptome assemblies from RNA-seq. *Nat Methods* 14: 68 – 70

Page MF, Carr B, Anders KR, Grimson A, Anderson P (1999) SMG-2 is a phosphorylated protein required for mRNA surveillance in Caenorhabditis elegans and related to Upf1p of yeast. *Mol Cell Biol* 19: 5943 – 5951

Park Y, Reyna-Neyra A, Philippe L, Thoreen CC (2017) mTORC1 balances cellular amino acid supply with demand for protein synthesis through post-transcriptional control of ATF4. *Cell Rep* 19: 1083 – 1090

Park Y, Reyna-Neyra A, Philippe L, Thoreen CC (2017) Gene Expression Omnibus GSE97384 (https://www.ncbi.nlm.nih.gov/geo/query/acc.cgi?acc=GSE97384). [DATASET]

Paz I, Kosti I, Ares Jr M, Cline M, Mandel-Gutfreund Y (2014) RBPmap: a web server for mapping binding sites of RNA-binding proteins. *Nucleic Acids Res* 42: W361 – W367

Pertea M, Pertea GM, Antonescu CM, Chang T-C, Mendell JT, Salzberg SL (2015) StringTie enables improved reconstruction of a transcriptome from RNA-seq reads. *Nat Biotechnol* 33: 290 – 295

Powell DR (2015) Degust: interactive RNA-seq analysis. https://doi.org/10.5281/zenodo.3258933

Pulak R, Anderson P (1993) mRNA surveillance by the *Caenorhabditis elegans* smg genes. *Genes Dev* 7: 1885 – 1897

Risso D, Ngai J, Speed TP, Dudoit S (2014) Normalization of RNA-seq data using factor analysis of control genes or samples. *Nat Biotechnol* 32: 896 – 902

Ritchie ME, Phipson B, Wu D, Hu Y, Law CW, Shi W, Smyth GK (2015) limma powers differential expression analyses for RNA-sequencing and microarray studies. *Nucleic Acids Res* 43: e47

Robinson MD, McCarthy DJ, Smyth GK (2009) edgeR: a Bioconductor package for differential expression analysis of digital gene expression data. *Bioinformatics* 26: 139 – 140

Schofield JA, Duffy EE, Kiefer L, Sullivan MC, Simon MD (2018) TimeLapse-seq: adding a temporal dimension to RNA sequencing through nucleoside recoding. *Nat Methods* 15: 221 – 225

Shen S, Park JW, Lu Z-X, Lin L, Henry MD, Wu YN, Zhou Q, Xing Y (2014) rMATS: robust and flexible detection of differential alternative splicing from replicate RNA-Seq data. *Proc Natl Acad Sci USA* 111: E5593 – E5601

Singh G, Rebbapragada I, Lykke-Andersen J (2008) A competition between stimulators and antagonists of Upf complex recruitment governs human nonsense-mediated mRNA decay. *PLoS Biol* 6: e111

Smith JE, Baker KE (2015) Nonsense-mediated RNA decay–a switch and dial for regulating gene expression. *BioEssays* 37: 612 – 623

Song MS, Salmena L, Pandolfi PP (2012) The functions and regulation of the PTEN tumour suppressor. *Nat Rev Mol Cell Biol* 13: 283 – 296

The Gene Ontology Consortium (2019) The Gene Ontology Resource: 20 years and still GOing strong. *Nucleic Acids Res* 47: D330 – D338

Thorvaldsdóttir H, Robinson JT, Mesirov JP (2013) Integrative Genomics Viewer (IGV): high-performance genomics data visualization and exploration. *Brief Bioinform* 14: 178 – 192

Toma KG, Rebbapragada I, Durand S, Lykke-Andersen J (2015) Identification of elements in human long 3' UTRs that inhibit nonsense-mediated decay. *RNA* 21: 887 – 897

UniProt Consortium (2021) UniProt: the universal protein knowledgebase in 2021. *Nucleic Acids Res* 49: D480 – D489

Van Nostrand EL, Freese P, Pratt GA, Wang X, Wei X, Xiao R, Blue SM, Chen J-Y, Cody NAL, Dominguez D *et al* (2020) A large-scale binding and functional map of human RNA-binding proteins. *Nature* 583: 711 – 719

Vitting-Seerup K, Sandelin A (2019) IsoformSwitchAnalyzeR: analysis of changes in genome-wide patterns of alternative splicing and its functional consequences. *Bioinformatics* 35: 4469 – 4471

Waldron JA, Tack DC, Ritchey LE, Gillen SL, Wilczynska A, Turro E, Bevilacqua PC, Assmann SM, Bushell M, Le Quesne J (2019) Gene Expression Omnibus. GSE134888 (https://www.ncbi.nlm.nih.gov/geo/query/acc.cgi?acc=GSE134888). [DATASET]

Waldron JA, Tack DC, Ritchey LE, Gillen SL, Wilczynska A, Turro E, Bevilacqua PC, Assmann SM, Bushell M, Le Quesne J (2019) mRNA structural elements immediately upstream of the start codon dictate dependence upon eIF4A helicase activity. *Genome Biol* 20: 1 – 23

Watson M, Park Y, Thoreen C (2021) Roadblock-qPCR: A simple and inexpensive strategy for targeted measurements of mRNA stability. *RNA* 27: 335 – 342

Wek RC (2018) Role of eIF2α Kinases in Translational Control and Adaptation to Cellular Stress. *Cold Spring Harb Perspect Biol* 10: a032870

Weng Y, Czaplinski K, Peltz SW (1998) ATP is a cofactor of the Upf1 protein that modulates its translation termination and RNA binding activities. *RNA* 4: 205 – 214

Yee BA, Pratt GA, Graveley BR, Van Nostrand EL, Yeo GW (2019) RBP-Maps enables robust generation of splicing regulatory maps. *RNA* 25: 193 – 204

Yepiskoposyan H, Aeschimann F, Nilsson D, Okoniewski M, Mühlemann O (2011) Autoregulation of the nonsense-mediated mRNA decay pathway in human cells. *RNA* 17: 2108 – 2118

Yi Z, Sanjeev M, Singh G (2021) The Branched Nature of the Nonsense-Mediated mRNA Decay Pathway. *Trends Genet* 37: 143 – 159

Young SK, Wek RC (2016) Upstream open reading frames differentially regulate gene-specific translation in the integrated stress response. *J Biol Chem* 291: 16927 – 16935

Young-Baird SK, Lourenço MB, Elder MK, Klann E, Liebau S, Dever TE (2020) Suppression of MEHMO syndrome mutation in eIF2 by small molecule ISRIB. *Mol Cell* 77: 875 – 886

Zünd D, Gruber AR, Zavolan M, Mühlemann O (2013) Translation-dependent displacement of UPF1 from coding sequences causes its enrichment in 3' UTRs. *Nat Struct Mol Biol* 20: 936 – 943

